Check for updates

EurJIC
European Journal of Inorganic Chemistry

Chemistry Europe
European Chemical Societies Publishing

Accepted Article

Title: Synthesis, Characterization and Electrochemical Properties of Tri- and Tetranuclear CoIII-Oxo Complexes

Authors: Timo Fockenberg, Niklas Sülzner, Hatem Amin, Christoph Wölper, Christof Hättig, and Stephan Schulz

This manuscript has been accepted after peer review and appears as an Accepted Article online prior to editing, proofing, and formal publication of the final Version of Record (VoR). The VoR will be published online in Early View as soon as possible and may be different to this Accepted Article as a result of editing. Readers should obtain the VoR from the journal website shown below when it is published to ensure accuracy of information. The authors are responsible for the content of this Accepted Article.

To be cited as: *Eur. J. Inorg. Chem.* **2025**, e202500170

Link to VoR: https://doi.org/10.1002/ejic.202500170

WILEY VCH

10.1002/ejic.202500170

WILEY VCH

RESEARCH ARTICLE

Synthesis, Characterization and Electrochemical Properties of Tri- and Tetranuclear Co^{III}-Oxo Complexes

Timo Fockenberg[a], Niklas Sülzner[b], Hatem M.A. Amin[a], Christoph Wölper[a], Christof Hättig[b], and Stephan Schulz[a,c]*

[a] T. Fockenberg, Dr. H. M. A. Amin, Dr. C. Wölper, Prof. S. Schulz*
Institute of Inorganic Chemistry
University of Duisburg-Essen
Universitätsstr. 5-7, 45141 Essen, Germany
E-mail: stephan.schulz@uni-due.de

[b] Dr. N. Sülzner, Prof. C. Hättig
Lehrstuhl für Theoretische Chemie
Ruhr-Universität Bochum
Universitätsstraße 150, 44780, Bochum, Germany

[c] Prof. S. Schulz*
Center for Nanointegration Duisburg-Essen (CENIDE)
University of Duisburg-Essen
Carl-Benz-Straße 199, 47057 Duisburg, Germany
E-mail: stephan.schulz@uni-due.de

Supporting information for this article is given via a link at the end of the document.

Abstract. Heterocubane-type complexes containing a central $[Co^{III}_4O_4]$ core have received increasing interest as surface cut-outs of active spinel-type Co_3O_4 water splitting catalysts. We here report the synthesis of a series of tetranuclear ($[Co_4O_4(O_2CR)_4(py)_4]$ (R = Me **1**, Et **2**, *n*-Pr **3**)) and trinuclear Co(III) carboxylate complexes $[Co^{III}_3(\mu_3\text{-}O)(\mu_2\text{-}OH)(O_2CR)_3(py)_5](NO_3)_2$ (R = *i*-Pr **4**, *t*-Bu **5**) and their structural (sc-XRD) and spectroscopic (except **5**, ^{1}H NMR, UV/Vis, IR) characterization. Quantum chemical calculations using density functional theory (DFT) showed that the relative stability of the tetranuclear complexes vs. the trinuclear complexes decreases with increasing steric demand of the carboxylate ligand. In addition, the UV/vis and IR spectra of the tetranuclear complexes were calculated to deconvolute contributions from the carboxylate ligands and the Co-oxo core. Furthermore, the electrochemical properties of the complexes **1**−**4** were studied by cyclic voltammetry (CV), demonstrating that the redox potential of the complexes correlates with the steric demand of the carboxylate ligand.

Introduction

Catalytic oxidation reactions play a pivotal role in chemical industry, where selectivity, yield, and efficiency are crucial for the viability of industrial chemical processes[1], as well as in academic research.[2,3] Extensive studies were performed in order to understand the catalytic mechanism in detail and, based on this knowledge, to enable the rational design of efficient using naturally abundant catalysts. Cobalt oxides are recognized as one of the most efficient, non-precious catalysts for industrially relevant oxidation catalysis. For example, spinel-type Co_3O_4 nanoparticles have been shown to be effective catalysts for heterogeneous oxidation reactions including water electrolysis and alcohol oxidation.[4–7] In such oxidation reactions, Co-O species with an oxidation state of +III or higher are assumed as the active sites,[8] but detailed mechanistic information is still lacking. To better understand the catalytic reaction mechanism and the nature of active species, molecular cluster compounds have received increasing attention as model systems for their heterogeneous counterparts. Molecular model systems allow a precise control of the chemical composition and, more importantly, the specific metal oxidation states, facilitating different spectroscopic analyses and computational studies, which is necessary to understand structure-activity correlations in more detail.[9–11]

Among others, heterocubane-type $[Co^{III}_4O_4]$ complexes have been intensively studied as persuasive model systems as they are structurally similar to a subunit of extended CoO_x and have a multi-metallic nature.[12,13] First

This article is protected by copyright. All rights reserved.

Accepted Manuscript

10990682c, ja, Downloaded from https://chemistry-europe.onlinelibrary.wiley.com/doi/10.1002/ejic.202500170 by Ruhr-Universität Bochum, Wiley Online Library on [04/06/2025]. See the Terms and Conditions (https://onlinelibrary.wiley.com/terms-and-conditions) on Wiley Online Library for rules of use; OA articles are governed by the applicable Creative Commons License

studies in 1998 by Beattie et al. on isolated homogeneous cobalt complexes revealed the formation of a variety of high-valent states of Co-oxo intermediates during oxidation reactions.[14] Das et al. established a high-yield method for the synthesis of $[Co^{III}_4O_4]$ heterocubane-type complexes[15] and also conducted extensive research on the thermal oxidation catalysis using different cobalt-oxo complexes. They demonstrated the catalytic activity of trimeric Co(III) complexes immobilized on chemically modified silica (CMS) for the selective aerobic oxidation of alkyl aromatics,[16] while heterocubane-type $[Co^{III}_4O_4]$ complexes were found to catalytically oxidize (with a given oxidant) α-pinene (O_2),[15] ethyl benzene and p-xylene (O_2),[17–19] as well as benzylic alcohols (TBHP(tert-Butyl hydroperoxide)).[20] Even higher selectivities and conversion rates were achieved by immobilization of these $[Co^{III}_4O_4]$ complexes on CMS, i.e., for the heterogeneous oxidation of benzyl alcohols and secondary aliphatic alcohols with THBP, [21] α-pinene with O_2 (air),[22] styrene with THBP and diphenyl methane with THBP, H_2O_2, or NaOCl, respectively.[23]

$[Co^{III}_4O_4]$ heterocubane-type clusters have also been used for the oxygen evolution reaction (OER) in alkaline media. Britt et al. and Nocera et al. demonstrated the reversible formation of tetravalent Co^{IV} in the one-electron oxidation product $[Co^{IV}Co^{III}_3O_4(OAc)_4(py)_4]^+$ by use of X-ray diffraction and EPR spectroscopy and reported that the properties of this state resembles that of the CoO_x film.[24,25] Nocera et al. and Tilley et al. also found indications for the involvement of higher Co oxidation states under OER conditions, presumably $[Co^{IV}_2Co^{III}_2O_4]$ or $[Co^{V}Co^{III}_3O_4]$.[9,26] Moreover, Tilley and co-workers reported that hydrocarbon C−H oxidation using $[Co_4O_4(OAc)_4(py)_4][BF_4]$ most likely occurs via concerted proton-electron transfer.[27] These examples showcase the suitability of $[Co_4O_4]$ heterocubane-type complexes for oxidation reactions.

Notably, the chemical and electronic properties of the $[Co_4O_4]$ complexes can be altered by modification of the organic substituents. Previous studies primarily focused on the para-functionalization of the pyridine ligand by use of alkyl, cyano, dimethylamino, methoxy, ester, halide, and vinyl groups with different steric and electronic properties.[18,20,28–33] Moreover, chelating ligands containing pyridine moieties were introduced, e.g., bi(2-pyridyl) ketone, 2,2'-bipyridine, 2-pyridone, 7-azaindole, 2-pyridinemethanol, 2,6-pyridinedimethanol, which allowed the variation of the pyridine to acetate ratio while the cubic $[Co^{III}_4O_4]$ core is preserved.[10–12,28,34,35] In contrast, the variation of the acetate (OAc) ligand was less studied and primarily focused on modifying the electronic properties of the ligand by introducing electron-withdrawing substituents, e.g., halides or benzoic acid derivatives (trifluoroacetate, 4-nitro/chlorobenzoate, chloro/bromo/methoxyacetic acid).[20,28,31,33] Propionic acid was used by Wang et al.,[31] but the resulting complex could not be fully characterized. In addition, pivalic acid was introduced by Das et al.,[36] but this sterically demanding carboxylate substituent yielded the trinuclear complex $[Co_3(\mu_3\text{-}O)(\mu_2\text{-}OH)(OAc)_5(py)_3]^+$, respectively. Structurally related trinuclear Co-oxo complexes were also previously reported.[14,37] Studies using mononuclear water oxidation catalysts (WOC) showed a correlation between catalytic activity and ligand size.[38–41] In addition, the electrochemical properties of $[Co^{III}_4O_4]$ heterocubane-type complexes were tuned by introducing electron-donating/withdrawing ligands, which were found to shift the redox couples cathodically/anodically in the cyclic voltammograms (CV).[28] We therefore became interested in developing a family of Co(III) carboxylate complexes with systematically increased ligand size to improve our knowledge on structure-reactivity relationships. Herein, we report the synthesis and characterization of a series of tetranuclear $[Co_4O_4(O_2CR)_4(py)_4]$ (R = Me **1**, Et **2**, *n*-Pr **3**) and trinuclear Co^{III} complexes $[Co^{III}_3(\mu_3\text{-}O)(\mu_2\text{-}OH)(O_2CR)_3(py)_5](NO_3)_2$ (R = *i*-Pr **4**, *t*-Bu **5**), respectively.

Results and Discussion

Synthesis and Structural Characterization

$[Co_4O_4(O_2CMe)_4(py)_4]$ (**1**), $[Co_4O_4(O_2CEt)_4(py)_4]$ (**2**), and $[Co_4O_4(O_2C\textit{n}\text{-}Pr)_4(py)_4]$ (**3**) were synthesized by reactions of $Co(NO_3)_2$ with two eq. of the corresponding sodium carboxylic acid and pyridine (py) in methanol (MeOH) and H_2O_2 using a slightly modified reaction protocol of Chakrabarty et al.[17] (Scheme 1).

$$Co(NO_3)_2 + 2\ NaOOCR + py \xrightarrow[-H_2O,\ -NaNO_3]{\substack{MeOH,\ H_2O_2\\ \Delta T,\ 4\ h}} [Co_4O_4(O_2CR)_4(py)_4]$$

R = Me (**1**), Et (**2**), *n*-Pr (**3**)

Scheme 1. Synthesis of the tetranuclear complexes **1**−**3**.

Complex **1** was purified by precipitation of a solution of **1** in dichloromethane (CH_2Cl_2, DCM) with petroleum ether and was obtained as a dark green powder. Complexes $[Co_4O_4(O_2CEt)_4(py)_4]$ (**2**) and $[Co_4O_4(O_2C\textit{n}\text{-}Pr)_4(py)_4]$ (**3**)

This article is protected by copyright. All rights reserved.

10990682c, ja, Downloaded from https://chemistry-europe.onlinelibrary.wiley.com/doi/10.1002/ejic.202500170 by Ruhr-Universitat Bochum, Wiley Online Library on [04/06/2025]. See the Terms and Conditions (https://onlinelibrary.wiley.com/terms-and-conditions) on Wiley Online Library for rules of use; OA articles are governed by the applicable Creative Commons License

Accepted Manuscript

were purified by column chromatography using a 2.5:1 mixture of cyclohexane (cHex) and ethanol (EtOH), respectively. The ^{1}H and ^{13}C NMR spectra of complexes **1**−**3** (Figure. S1, S2, S5, S6, S9, S10 Supporting Information (SI)) show the expected resonances of the carboxylate unit (**Table *1***). Unfortunately, all attempts to further increase the carbon chain length by using the sodium salts of caproic and valeric acids were unsuccessful, since no defined product could be isolated from the resulting resin-like product mixtures. We therefore introduced branched carboxylate ligands by using sodium salts of *iso*-butyric acid and pivalic acid in order to further increase the steric demand of the carboxylate ligand (**Scheme**), resulting in the formation of trinuclear complexes $[Co^{III}_3(\mu_3\text{-}O)(\mu_2\text{-}OH)(O_2CR)_3(py)_5](NO_3)_2$ (R = *i*-Pr **4**, *t*-Bu **5**), respectively.

$$Co(NO_3)_2 + 2\ NaOOCR + py \xrightarrow[-H_2O,\ -NaNO_3]{MeOH,\ H_2O_2,\ \Delta T,\ 4\ h} [Co^{III}_3(\mu_3\text{-}O)(\mu_2\text{-}OH)(O_2CR)_3(py)_5](NO_3)_2$$

R = *i*-Pr (**4**), *t*-Bu (**5**)

Scheme 1. Synthesis of the trinuclear complexes **4** and **5**.

A pure sample of complex **4** was obtained after washing with THF (Tetrahydrofuran). The ^{1}H-NMR spectrum of complex **4** (CH_3CN-d^3, Figure S13) showed resonances of the carboxylate ligand at 2.96 and 2.70 ppm ($O_2CCH\mathit{Me}_2$, ration of 1:2) and three doublets between 1.05 and 1.15 ppm ($O_2CCH\mathit{Me}_2$) as well as three resonances for the coordinating pyridine ligands in the ratio 1:2:2 with overlapping signals at 8.01 and 7.54 ppm, respectively. In addition, resonances at 1.44 ppm were assigned to the OH protons. Unfortunately, complex **5** always formed as minor component together with the known complex $[Co^{III}_3(\mu_3\text{-}O)(\mu_2\text{-}OH)(O_2C\mathit{t}\text{-}Bu)_5(py)_3]$.[36] Despite several attempts, we failed to isolate complex **5** in its pure form, hence this compound could not be spectroscopically characterized in detail. However, its crystal structure was determined by sc-XRD using a hand-picked crystal.

Table *1.* ^{1}H- and ^{13}C-NMR resonances [ppm] of the carboxylate ligands in complexes **1**−**3**.

Complex	NMR	OO***C***	***CH*₃**	***CH*₂CH₃**	***CH*₂CH₂CH₃**
1[a]	^{1}H	-	2.15	-	-
2	^{1}H	-	1.06	2.38	-
3	^{1}H	-	0.88	1.57	2.34
1	^{13}C	188.8	25.6	-	-
2	^{13}C	192.0	9.5	32.6	-
3	^{13}C	191.4	13.3	19.1	41.5

[a] The ^{1}H resonances of complex **1** (Figure S1) are systematically shifted to higher field by 0.1 ppm with respect to the resonances reported in the literature[19] due to a different referencing.

Single crystal X-ray diffraction (sc-XRD)

Single crystals of the known complex **1**, which co-crystallized with five DCM molecules in the unit cell,[14,17,19,21] and the new complexes **2** and **3** suitable for sc-XRD were obtained by slow vapor diffusion of *n*-hexane into solutions of **1**−**3** in DCM. Complexes **2** (Figure**Figure 1**a) and **3** (**Figure 1**b) crystallize in the monoclinic space group 14 (settings $P2_1/n$ and $P2_1/c$, respectively) with one molecule per asymmetric unit accompanied by solvent molecules. Central bond lengths and angles of complexes **1**−**3** and of additional tetranuclear complexes with a central $[Co^{III}_4O_4]$ core are summarized in **Table 2**.[14,20,28]

This article is protected by copyright. All rights reserved.

10990682c, ja, Downloaded from https://chemistry-europe.onlinelibrary.wiley.com/doi/10.1002/ejic.202500170 by Ruhr-Universität Bochum, Wiley Online Library on [04/06/2025]. See the Terms and Conditions (https://onlinelibrary.wiley.com/terms-and-conditions) on Wiley Online Library for rules of use; OA articles are governed by the applicable Creative Commons License

Accepted Manuscript

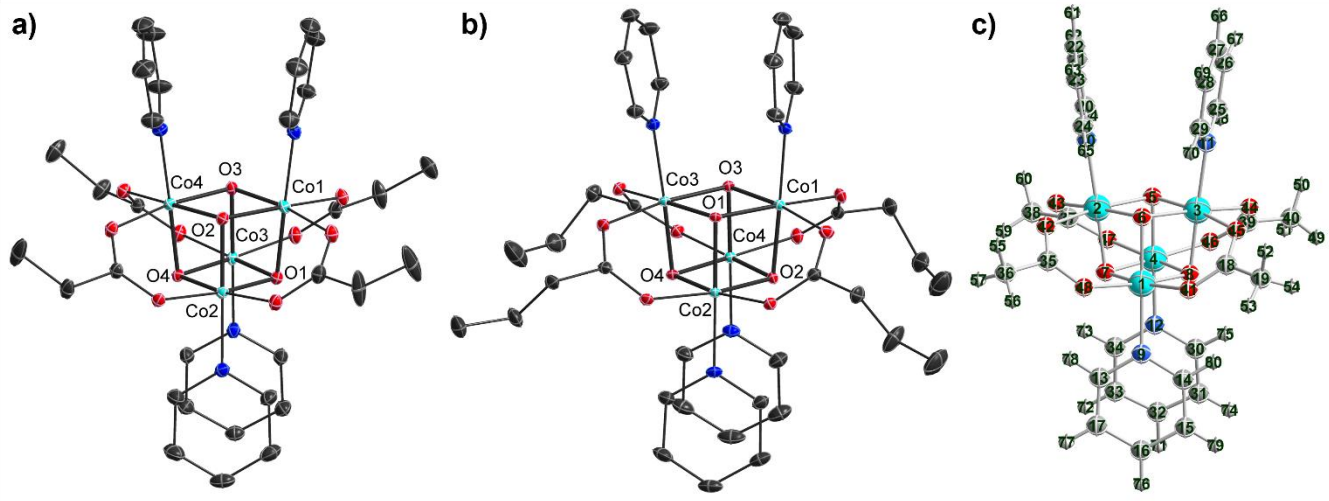


Figure 1. Single crystal X-ray structures (H atoms not shown) of **a)** $[Co_4O_4(O_2CEt)_4(py)_4]$ (**2**) and **b)** $[Co_4O_4(O_2Cn\text{-}Pr)_4(py)_4]$ (**3**). Displacement ellipsoids are displayed at 50% probability levels. **c)** Optimized structure of **1** (H atoms shown) including atom numbering at the DFT/PBE0/def2-TZVP level of theory. Color coding: Co light blue; O red; N blue; C gray; H white.

Table 2. Central bond lengths (Å) and angles (°) within the $[Co_4O_4]$ core of complexes **1**−**3** and of structurally related complexes $[Co_4O_4(O_2CPh)_4(py)_4]$[20] (**I**) and $[Co_4O_4(O_2C_2F_3)_4(py)_4]$[28] (**II**)

Complex	**Co-(μ^3-O)**	**Co−O−Co**[a]	**O−Co−O**[a]	**Co−N_{Py}**	**Co−O_{O2C}**
1[14]	1.874(2)-1.890(2)	92.35(9)-98.67(10)	81.25(9)-86.99(9)	1.966(3)-1.971(3)	1.955(2)-1.984(2)
2	1.8574(12)-1.8761(12)	91.98(5)-98.38(5)	81.57(5)-87.06(5)	1.9486(14)-1.9647(15)	1.9468(13)-1.9629(12)
3	1.8616(14)-1.8700(15)	92.44(6)-97.94(7)	82.08(6)-87.04(6)	1.9505(18)-1.9590(18)	1.9358(15)-1.9815(15)
I[20]	1.874(4)-1.890(4)	92.35(9)-98.67(10)	81.25(9)-86.99(9)	1.966(4)-1.971(5)	1.955(4)-1.984(4)
II[28]	1.858(2)-1.869(2)	92.98(9)-98.16(9)	81.82(9)-86.42(9)	1.953(3)	1.969(2)-1.979(2)

[a] Bond angles within the Co_4O_4 core.

The O and Co atoms alternately occupy the corners of a distorted cube, in which the Co-O-Co bond angles are larger, and the O-Co-O angles are smaller than 90° (see **Table 2**). The arrangement can be described as a Co_4 tetrahedron with μ_3-bridging oxide anions on its faces. Each Co atom is further coordinated by one neutral pyridine ligand, while each carboxylic ligand serves as μ_2-bridging unit and coordinates to two Co atoms. The Co−O bond lengths within the cubic $[Co^{III}_4O_4]$ core are almost independent from the size of the carboxylic ligand, whereas a steady decrease of the O−Co−O and steady increase of the Co−O−Co bond angles within $[Co^{III}_4O_4]$ with increasing steric demand of the carboxylate ligands is observed.

Single crystals of the trinuclear complexes **4** and **5** were obtained by slow vapor diffusion of *n*-hexane into solutions of **4** and **5** in THF. Complexes **4** and **5** crystallize with two nitrate counter ions and one THF solvent molecule per asymmetric unit in monoclinic (**4**, $P2_1/c$) and orthorhombic (**5**, $P2_12_12_1$) space groups, respectively. Additional solvent molecules in **5** could not be modelled n were removed with SQUEEZE.

This article is protected by copyright. All rights reserved.

10990682c, ja, Downloaded from https://chemistry-europe.onlinelibrary.wiley.com/doi/10.1002/ejic.202500170 by Ruhr-Universitat Bochum, Wiley Online Library on [04/06/2025]. See the Terms and Conditions (https://onlinelibrary.wiley.com/terms-and-conditions) on Wiley Online Library for rules of use; OA articles are governed by the applicable Creative Commons License

Accepted Manuscript

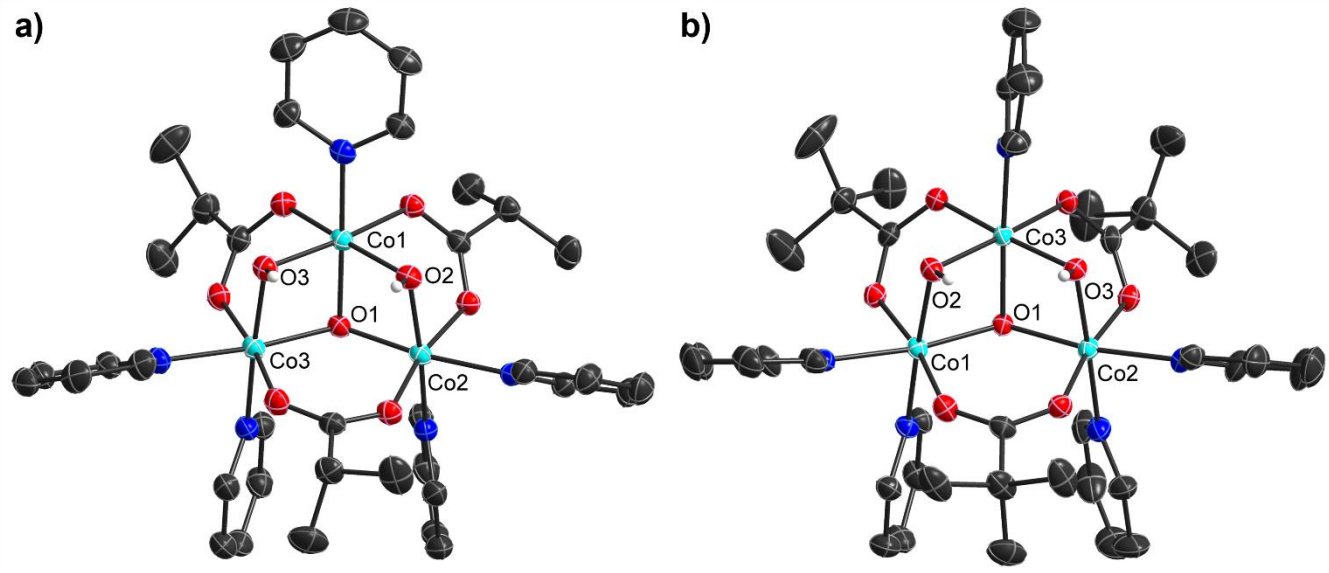


Figure 2. Molecular structures of **a)** $[Co^{III}_3(\mu_3\text{-}O)(\mu_2\text{-}OH)(O_2C\textit{i}\text{-}Pr)_3(py)_5](NO_3)_2$ (**4**) and **b)** $[Co^{III}_3(\mu_3\text{-}O)(\mu_2\text{-}OH)(O_2C\textit{t}\text{-}Bu)_3(py)_5](NO_3)_2$ (**5**) in the solid state. Nitrate counter anions, solvent molecule, minor comonents of disordered parts and H omitted for clarity except for the OH protons. Color coding: Co light blue; O red; N blue; C gray; H white. Displacement ellipsoids are displayed at 50% probability levels, H atoms as spheres of arbitray radii.

The central bond lengths within the trinuclear $[Co^{III}_3(\mu_3\text{-}O)(\mu_2\text{-}OH)]$ core and to the coordinating ligands are summarized in **Table 3**. Complex **4** and **5** are furthermore compared to the known trinuclear complex **III** with $[Co^{III}_3(\mu_3\text{-}O)(\mu_2\text{-}OH)]$ core reported by Sumner et al.[38] No significant differences in the bond lengths and angle of the central cores can be found.

Table 3. Central bond lengths [Å]) within the $[Co^{II}I_3(\mu_3\text{-}O)(\mu_2\text{-}OH)]$ core of complexes **4** and **5** as well as the dication $[Co^{III}_3(\mu_3\text{-}O)(\mu_2\text{-}OH)(OAc)_3(py)_5]^{2+}$ (**III**).[38]

Complex	**Co-(μ^3-O)**	**Co-(μ^2-OH)**	**Co−N_{Py}[a]**	**Co−N_{Py}[b]**	**Co−O_{O2C}**
4	1.8631(15)-1.8772(15)	1.8858(16)-1.9112(16)	1.953(2)-1.9578(19)	1.9931(19), 2.002(2)	1.8941(16) - 1.9156(16)
5	1.8806(18)-1.8903(16)	1.8796(19)-1.9001(19)	1.945(2)-1.964(2)	1.987(2), 1.996(2)	1.8848(19)-1.9121(19)
III[38]	1.862(3)-1.892(4)	1.880(4)-1.906(4)	1.929(5)-1.962(6)	1.983(5), 1.990(4)	1.882(3)-1.909(3)

[a] Co-N_{Py} distances vertical pyridine in Figure**Figure 2**. [b]Co-N_{Py} distances horizontal pyridine in Figure**Figure 2**.

Structure Optimizations

The structure of complex **1** was optimized by quantum chemical calculation using density functional theory (DFT) for the isolated cluster in vacuum (see Figure 1c). Even without symmetry constraints, the structure reveals near S_4 symmetry, allowing for a simple re-optimization in this point group. As symmetry will be important for many comparisons between experiment and theory in the following sections, a few aspects in this regard should be highlighted.

The neat $[Co^{III}_4O_4]^{4+}$ core without ligands or e.g. a hypothetical $[Co_4O_4(O_2CH)_6]^{2-}$ complex containing six formate ($OCHO^-$) ligands would have T_d (tetrahedral) symmetry. Substitution of two of these formate ligands by four linear N-donor ligands like HCN, as in the complex $[Co_4O_4(O_2CH)_4(HCN)_4]$, already reduces the symmetry to D_{2d}. Finally, substitution of the formate by acetate ligands, which lack axial symmetry, and/or HCN by pyridine, which prefers a tilted conformation, reduces the overall symmetry to S_4 for $[Co_4O_4(OAc)_4(py)_4]$ (**1**). These considerations will be helpful for the understanding of the UV/Vis and IR spectra and their comparisons with spectra for more symmetric model systems (*vide infra*).

This article is protected by copyright. All rights reserved.

10990682c, ja, Downloaded from https://chemistry-europe.onlinelibrary.wiley.com/doi/10.1002/ejic.202500170 by Ruhr-Universität Bochum, Wiley Online Library on [04/06/2025]. See the Terms and Conditions (https://onlinelibrary.wiley.com/terms-and-conditions) on Wiley Online Library for rules of use; OA articles are governed by the applicable Creative Commons License

The near tetrahedral symmetry is also reflected in structural parameters such as the Mayer bond indices (MBIs) as calculated here for $[Co_4O_4(OAc)_4(py)_4]$ **1** (see **Table *4***) to characterize the chemical bonding in this complex. In the following discussion, the S_4 axis is assumed to be oriented along the longer, vertical axis, defined as the *z* axis and in accordance with **Figure 1**c. First, the $[Co^{III}_4O_4]$ core itself is considered. Due to the reduction of the ideal T_d symmetry to S_4, only the atom pairs Co2/Co3 and Co1/Co4 are equivalent, but not necessarily the atoms within these pairs. Thus, there are three sets of Co−Co and Co−O bond lengths. There is moderate covalent Co−O bonding, as indicated by values of ≈0.6. The bond indices for Co2/O5 (0.64) and Co2/O6 (0.63) are almost identical, while that for Co2/O7 bond (0.60) is marginally smaller, in line with the fact that the $[Co^{III}_4O_4]$ core is slightly stretched along the *z* axis.

Table *4*. Calculated Mayer bond indices for the $[Co^{III}_4O_4]$ core and the acetate and pyridine ligands of complex **1**. Only values for symmetry inequivalent bonds are given. For atom numbering see Figure 1c

$[Co^{III}_4O_4]$ core			acetate			pyridine		
Atom 1	**Atom 2**	**MBI**	**Atom 1**	**Atom 2**	**MBI**	**Atom 1**	**Atom 2**	**MBI**
Co2	O5	0.64	C18	O41	1.53	N10	C24	1.41
Co2	O6	0.63	C18	O45	1.53	C24	C23	1.40
Co2	O7	0.60	C18	C19	0.98	C23	C22	1.43
Co2	N10	0.58	C19	H52	0.97	C22	C21	1.43
Co2	O42	0.50	C19	H53	0.98	C21	C20	1.40
Co2	O43	0.50	C19	H54	0.95	C20	N10	1.39
						C24	H65	0.96
						C23	H63	0.96
						C22	H61	0.96
						C21	H62	0.96
						C20	H64	0.95

Regarding the structure of the ligands, the MBIs confirm a delocalized three-center π bond (MBI ≈ 1.5) in the carboxylate groups and three mostly equivalent C-H bonds in the methyl group of acetate as well as a local C_{2v} symmetry of pyridine with the typical bond alteration (due to the perturbation by the N atom when compared to benzene). However, analysis of the MBIs indicates moderate covalent bonds between Co in the core and the ligands, i.e., to N in pyridine (0.58) and to O in the carboxylate (0.5), presumably with some ionic character.

Due to the similarity of **1** to the larger tetranuclear complexes **2** and **3** as well as the lower symmetry (C_s) of the trinuclear complexes **4** and **5**, the MBIs of these complexes have not been further investigated. Only exemplarily, some differences in the MBIs of the trinuclear complex **III** (Table S3) compared to the tetranuclear complex **1** (both with acetate ligands) are worth highlighting. The covalent character of the bonds between the Co atoms and the ligands is increased in **III** (Co-O(acetate) > 0.5; Co-N(pyridine) > 0.6), while that the MBIs for the bonds in the remaining $[Co^{III}_3(\mu_3\text{-}O)(\mu_2\text{-}OH)]$ core (ca. 0.6) are similar to that of $[Co_4O_4]$ without pronounced anisotropy. The O-H bonds of the μ-OH ligands are found to be slightly weakened compared to an isolated OH^- (0.87).

Stability Analysis

Since the synthesis of tetranuclear complexes with branched carboxylate ligands remained unsuccessful, the relative stability of the tetranuclear vs. trinuclear complexes has been analyzed using DFT calculations. We consider the conversion of the trinuclear $[Co_3O(OH)_2]$ into the tetranuclear $[Co_4O_4]$ species according to

This article is protected by copyright. All rights reserved.

10990682c, ja, Downloaded from https://chemistry-europe.onlinelibrary.wiley.com/doi/10.1002/ejic.202500170 by Ruhr-Universitat Bochum, Wiley Online Library on [04/06/2025]. See the Terms and Conditions (https://onlinelibrary.wiley.com/terms-and-conditions) on Wiley Online Library for rules of use; OA articles are governed by the applicable Creative Commons License

Accepted Manuscript

$$4\,[\mathrm{Co}_3^{+\mathrm{III}}(\mu_3\text{-}\mathrm{O})(\mu_2\text{-}\mathrm{OH})_2(\mathrm{O_2CR})_3(\mathrm{L})_5]^{2+} \rightleftharpoons 3\,[\mathrm{Co}_4^{+\mathrm{III}}(\mu_3\text{-}\mathrm{O})_4(\mathrm{O_2CR})_4(\mathrm{L})_4] + 8\,\mathrm{L} + 8\,\mathrm{H}^+ \quad (1)$$

whose Gibbs free reaction energy (in solution) is given by

$$\Delta(\Delta G) = \Delta G(\mathrm{R_2}) - \Delta G(\mathrm{R_1}) \quad (2)$$

$$3[G(\mathrm{Co_4O_4};\mathrm{R_2}) - G(\mathrm{Co_4O_4};\mathrm{R_1})] - 4[G(\mathrm{Co_3O(OH)_2};\mathrm{R_2}) - G(\mathrm{Co_3O(OH)_2};\mathrm{R_1})]$$

depending only on the total Gibbs free energies of the $[Co_3O(OH)_2]$ and $[Co_4O_4]$ species, but not the free (pyridine) ligand L or H^+.

Table *5*. Relative Gibbs free energies in solution (kJ mol^{-1}) for the interconversion from a trinuclear ($[Co^{III}_3(\mu_3\text{-}O)(\mu_2\text{-}OH)(O_2CR)_3(py)_5]^{2+}$) into a tetranuclear ($[Co_4O_4(O_2CR)_4(py)_4]$) complex according to eq. (2) for different carboxylate ligands (O_2CR) relative to formate (R = H) in methanol. Please notice that the values in other solvents differ (see Table S4 for Et_2O, THF, and cyclohexane).

R	Complex	Relative Stability (kJ mol^{-1})
H	—	0
Me	**III**	-103
***i*-Pr**	**4**	-51
***t*-Bu**	**5**	-38

As can be seen in **Table *5***, the position of the trinuclear ($[Co^{III}_3(\mu_3\text{-}O)(\mu_2\text{-}OH)]$) vs. tetranuclear ($[Co_4O_4]$) equilibrium lies in the case of acetate (R = Me) relative to formate (R = H) more than 100 kJ/mol on the tetranuclear site in the polar solvent methanol (MeOH). Increasing the steric demand at the carboxylate group by using iso-butyrate (R = *i*-Pr) results in a shift of the equilibrium position by ca. 50 kJ/mol toward the trinuclear complex, and further increase of the steric demand (R = *t*-Bu, pivalate) results in an additional shift of ca. 13 kJ/mol. The calculations demonstrate the relative destabilization of the tetranuclear species by increasing the steric demand of the carboxylate ligand, facilitating the formation of the trinuclear species. This trend is also more pronounced when pyridine is replaced by HCN as a model ligand, since the Δ*G* value becomes even positive for R = *t*-Bu relative to R = H (see Table S4).

Spectroscopic Characterization.

The IR spectra of the complexes **1**−**3** (Figure S3, S7, S11) are almost identical. All complexes exhibit four intense absorption bands below 800 cm-1 in accordance with comparable complexes, which also possess four intense IR absorption bands(~760–570 cm-1).[17] While the absorption band at ~760 cm^{-1} results from ring-based vibrations of the pyridine ring, the other three intense bands are tentatively assigned to characteristic vibrations of the heterocubane-type $[Co^{III}_4O_4]$ core. The band at ~630 cm^{-1} represents the typical Co−O stretching vibration[17] and was also observed in structurally related trinuclear $M_3(\mu_3\text{-}O)$ (with M= Co or Mn) complexes[42] as well as in a comparable Mn_4O_4 complex.[43]

We also used DFT to compute the IR absorption spectrum of **1** in vacuum. A comparison of the experimental IR spectra in acetonitrile solution (CH_3CN) and solid state (crystal) shows a good agreement with respect to the peak positions of the different vibrational modes (Figure**Figure 3**). However, the intensity of the two dominant bands around 1500 cm^{-1} was found to decrease relative to the intensity of the signals in the 500–1000 cm^{-1} region in the solid state compared to solution. This difference in the intensity ratios hints toward packing effects in the solid phase, preventing volume-expensive molecular vibrations, which is also in line with the opposite intensity ratios of these groups of signals in the calculated IR spectrum (in vacuum). Still, these main features can be said to be qualitatively reproduced by the calculations (*vide infra*).

This article is protected by copyright. All rights reserved.

10990682c, ja, Downloaded from https://chemistry-europe.onlinelibrary.wiley.com/doi/10.1002/ejic.202500170 by Ruhr-Universitat Bochum, Wiley Online Library on [04/06/2025]. See the Terms and Conditions (https://onlinelibrary.wiley.com/terms-and-conditions) on Wiley Online Library for rules of use; OA articles are governed by the applicable Creative Commons License

Accepted Manuscript

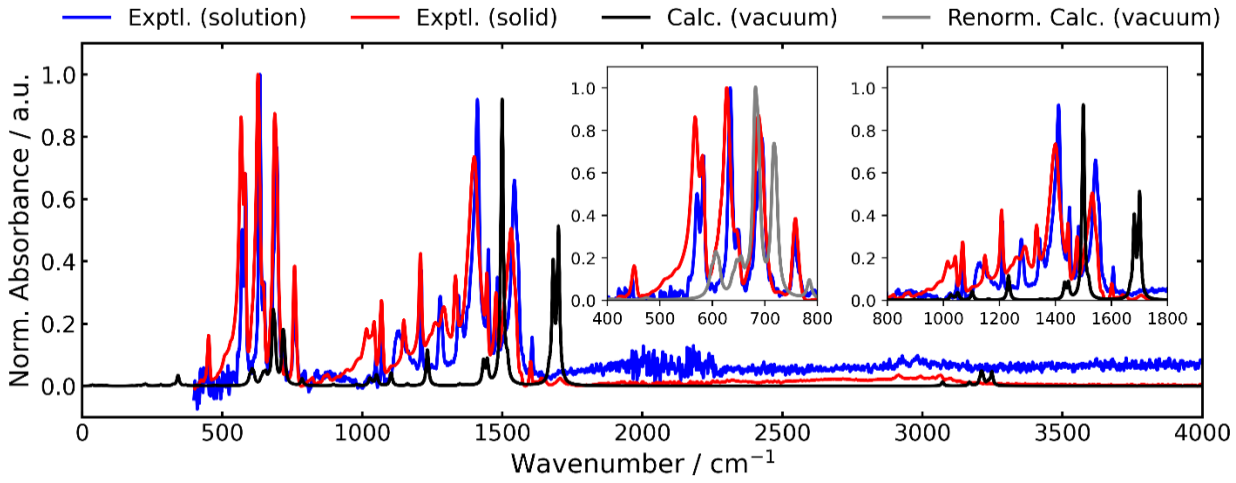


Figure 3. Comparison of the experimental IR absorption spectra in the solid (crystal) and solution (acetonitrile) phase and the calculated harmonic vibrational spectrum of **1** (S_4 symmetry) in vacuum at the tight PBE0/def2-TZVP level of theory.

The calculated IR spectrum successfully reproduces the main characteristic and most intense features of the experimental spectrum (**Figure 3**), *i.e.*, the [$Co^{III}_4O_4$] signals (500–1000 cm^{-1}) and the two intense groups around 1500 cm^{-1}. Despite a clear spectral shift between the calculated and experimental spectra, no attempts of scaling the harmonic frequencies have been undertaken. This shift and the missing signals in higher wavenumbers can be partly explained due to the ATR method. In difference to transmission IR, ATR-IR depends on the refractive index. This leads to a dependence of the intensity and shift of the IR signals on the latter. In ATR-IR the peak intensities and width increase with decreasing wavenumbers.[44]

Normal mode analysis of the vibrations allows us to dissect the total IR absorption spectrum of **1** into different contributions (FigureFigure **4**). Main signals in the region above 3000 cm^{-1} originate from the aromatic C–H stretching vibrations of the pyridine ligands (3070/3170/3210/3250 cm^{-1}), with the signals of the aliphatic C–H stretches from the CH_3 group of the acetate ligand (3000 cm^{-1}) being sub-ordinate. In contrast, the region between 1000 cm^{-1} and 2000 cm^{-1} is dominated by the symmetry-allowed combinations of the symmetric (1500 cm^{-1}) and asymmetric (1680/1700 cm^{-1}) C–O stretching vibrations of the carboxylate groups in the acetates, in good agreement with the experimental spectra.

The region below 1000 cm^{-1}, particularly between 500 cm^{-1} and 1000 cm^{-1}, is most interesting as it contains the characteristic signals from the [$Co^{III}_4O_4$] core. Whereas the total spectrum in this region has five apparent main bands (ca. 610/650/680/720/785 cm^{-1}), only two of these can be ascribed to the [$Co^{III}_4O_4$] core. The first band around 610 cm^{-1} consists of a two-fold degenerate *E* mode at 606 cm^{-1} and a *B* mode at 612 cm^{-1} (Table S5), while the second band at 680 cm^{-1} consists of an E mode at 681 cm^{-1} and a B mode at 687 cm^{-1}; originating from twisting/bending and wagging motions of the [$Co^{III}_4O_4$] core. In particular, a comparison with additional model systems with higher symmetry (Figure S17) showed that these two groups of signals would ideally belong to a dipole-allowed triply degenerate T_2 mode in the T_d point group. The other signals at 650 cm^{-1} and 710 cm^{-1} refer to (i) a collective motion and (ii) two individual, energetically close vibrations of the pyridine and acetate ligands, respectively. A detailed assignment of the 12 main localized vibrational modes and a comparison with the [$Co_4O_4(O_2CH)_4(HCN)_4$] (D_{2d}) and [$Co_4O_4(O_2CH)_6]^{2-}$ (T_d) model systems is given in Table S2. In direct comparison with the experiments (**Figure 3**), the bands in the calculated spectra appear to be shifted by about 30-40 cm^{-1} in this region. The two signals of the pyridine ligands are reproduced (720/785 cm^{-1}), while the frequency splitting between the *B* and *E* contributions of the [$Co^{III}_4O_4$] core modes appears to be larger in the experimental spectra. Besides, the collective mode of the acetate and pyridine ligands appears to be missing in the experimental spectra, presumably due to packing effects that suppress this mode and lower its transition dipole moment. Finally, the only relatively intense signal in the region below 500 cm^{-1} refers to a collective vibration of the core and its ligands.

This article is protected by copyright. All rights reserved.

10990682c, ja, Downloaded from https://chemistry-europe.onlinelibrary.wiley.com/doi/10.1002/ejic.202500170 by Ruhr-Universitat Bochum, Wiley Online Library on [04/06/2025]. See the Terms and Conditions (https://onlinelibrary.wiley.com/terms-and-conditions) on Wiley Online Library for rules of use; OA articles are governed by the applicable Creative Commons License

Accepted Manuscript

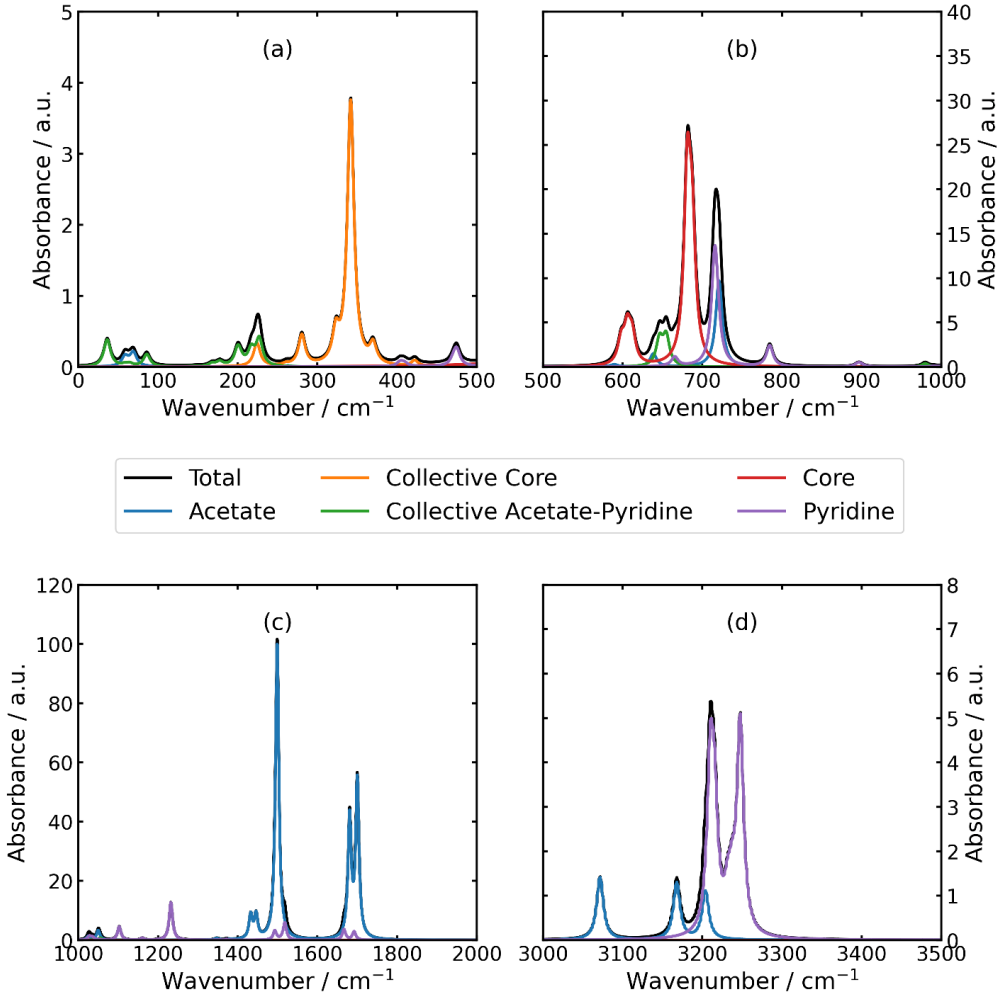


Figure 4. Decomposition of the calculated vacuum IR absorption spectrum of **1** into contributions from the ligands and the Co-oxo core.

The experimental and calculated IR spectra of the trinuclear complex **4** (Figure S18) also agree well. The most intense features in the experimental spectrum below 2000 cm^{-1} (e.g., the symmetric and asymmetric carbonyl stretching) are reproduced well despite small shifts and different intensity ratios as was observed for complex **1**. We also performed an analysis to dissect the vibrational spectrum into different contributions from the ligands and the core (Figure S19). Signals corresponding to the carboxylate and pyridine ligands are, unsurprisingly, very similar to those of complex **1.** In contrast, complex **4** is expected to show a high-frequency O–H stretch mode above 3000 cm^{-1}. Most interesting are the differences in the 500–1000 cm^{-1} region, where the characteristic contributions from the [Co^{III}_3(μ_3-O)(μ_2-OH)] core are located. Compared to the tetranuclear complex **1**, the trinuclear complex **4** reveals a more complex structure with (at least) nine (550/600/650/685/720/740/790/870/950 cm^{-1}) instead of five apparent bands. Only six of these bands are characteristic for the Co-oxo core, while the signals at 650 cm^{-1} (carboxylate) and 720/790 cm^{-1} (pyridine) stem from the ligands. The trinuclear [Co^{III}_3(μ_3-O)(μ_2-OH)] core differs from being just a corner of the [Co_4O_4] core due to protonation of two μ_3-O groups to μ-OH groups and a higher ratio of pyridine to carboxylate ligands. The resulting lower symmetry leads to a splitting of the signals. The three absorption bands with highest frequency (740/870/950 cm^{-1}) originate from symmetric and asymmetric bending modes of the μ-OH ligand, and the wagging vibration at 550 cm^{-1} also has large contributions from the μ-OH ligand. Characteristic for the central μ_3-O atom are the vibrations at 600 and 685 cm^{-1}, which are also observed for the tetranuclear complex **1**. A detailed assignment of the vibrational modes characteristic for the [Co^{III}_3(μ_3-O)(μ_2-OH)] core is given in Table S6.

The experimental UV/Vis absorption spectra of **1** in acetonitrile (Figure S4) reveal three characteristic features: a) a very weak $\epsilon_{630nm} = 0.042 \frac{L}{mmol*cm}$ shoulder around 630 nm, b) a more intense peak $\epsilon_{362nm} = 0.874 \frac{L}{mmol*cm}$ at ca. 362 nm, and c) a very intense $\epsilon_{253nm} = 2.088 \frac{L}{mmol*cm}$ signal below 253 nm. Time-dependent density functional theory (TDDFT) calculations reproduced features (1) and (2) but failed for feature (3).

This article is protected by copyright. All rights reserved.

10990682c, ja, Downloaded from https://chemistry-europe.onlinelibrary.wiley.com/doi/10.1002/ejic.202500170 by Ruhr-Universitat Bochum, Wiley Online Library on [04/06/2025]. See the Terms and Conditions (https://onlinelibrary.wiley.com/terms-and-conditions) on Wiley Online Library for rules of use; OA articles are governed by the applicable Creative Commons License

10.1002/ejic.202500170

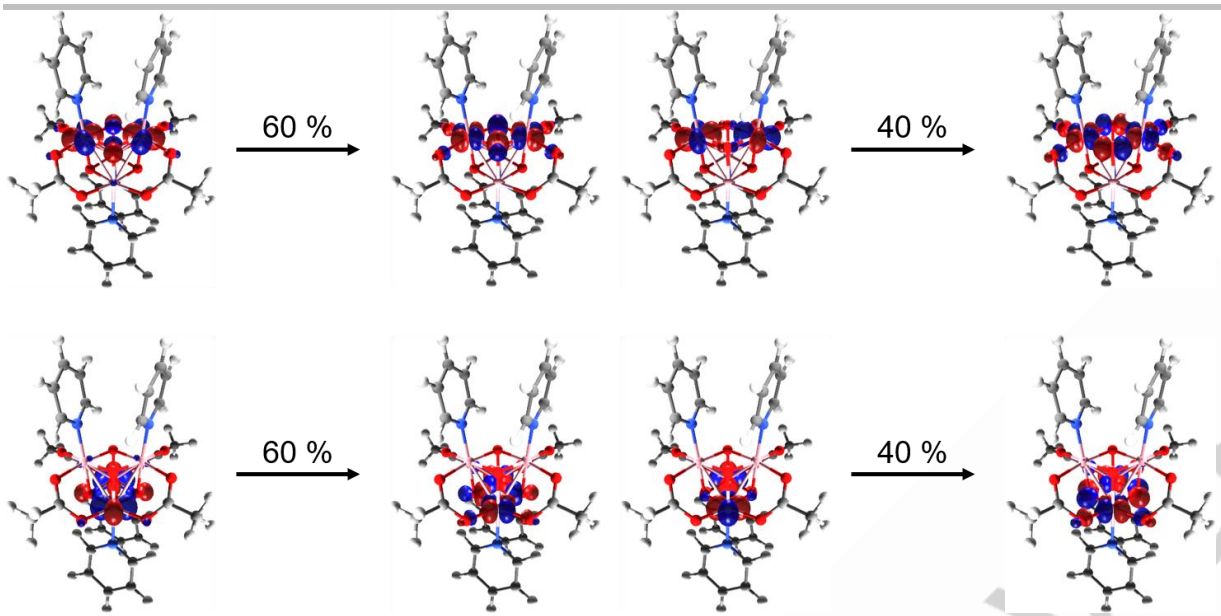


Figure 5. NTOs for the two transitions into the degenerate 1 ^{1}E state with d-d character.

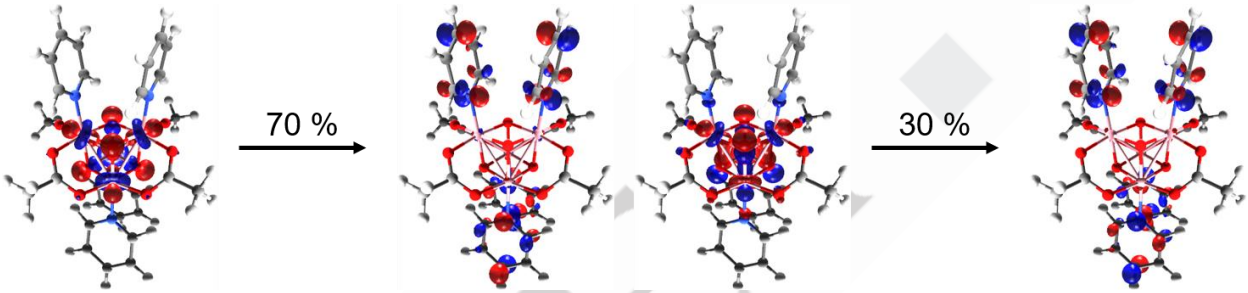


Figure 6. NTOs for the transition into the 8 ^{1}B state with MLCT character.

The calculations reveal a set of lowest-energy transitions with weak oscillator strengths (f): from the (totally symmetric) singlet ground (X = 1 ^{1}A) state into the 1 ^{1}E state at 607 nm (2.04 eV, f = 2 x 10^{-3}), the 2 ^{1}E state at 576 nm (2.15 eV, f = 0.2 x 10^{-3}), and the 3 ^{1}E state at 562 nm (2.21 eV, f = 0.3 x 10^{-3}). According to the natural transitions orbitals (NTOs) in **Figure 5** and S21-S22, these transitions can be characterized as d-d transitions, in line with the previous assignment of feature (1) at 630 nm feature in the experimental spectrum.[17,19] Moreover, a second, similarly weak transition into the 4 ^{1}B state around 419 nm (2.96 eV, f = 2 x 10^{-3}) with d/p-d/p character (Figure S23) appears in the experimental spectrum as an additional shoulder around 500 nm. Lastly, signal (2) from the experimental spectrum at 370 nm can be assigned to a metal-to-ligand charge-transfer (MLCT) transition, corresponding to the 8 ^{1}B state (284 nm, 4.40 eV, f = 0.1), which fits well to the postulated MLCTs of the μ_3-O-Co^{III} (355 nm) and the carboxylate-O-Co^{III} unit (250 nm),[19] respectively. The corresponding NTOs are shown in **Figure 6**. This assignment of the experimental features (1) and (2) has further been verified by an additional comparison with model systems (Figure S24), demonstrating that the rather intense d-d transitions, including feature (1), are not affected by the solvent or the carboxylate ligand, but change with the N-donor ligand. In contrast, the MLCT state does show a blue shift and is absent if the pyridine ligand is replaced by the simple HCN ligand.

Electrochemical Properties

A few studies have been devoted to the synthesis and catalytic application of tetranuclear heterocubane-type complexes containing a [$Co^{III}_4O_4$] core, however, data on their redox properties, despite their importance for catalysis, is largely lacking. It has been reported that the redox potentials of such tetranuclear complexes are directly correlated to their ligand environment.[28] We therefore investigated the influence of the carboxylate ligand size on the redox properties of complexes **1**–**3**. The cyclic voltammograms of complexes **1**−**3** are shown in Figure 6a over the potential range of 0-1.68 V vs. Fc/Fc^+ and in the narrower potential range around peak E1 in Figure 6b**.** All complexes revealed two (quasi)reversible redox peaks: E1 centered at 0.3 V, which can be assigned to the

This article is protected by copyright. All rights reserved.

10990682c, ja, Downloaded from https://chemistry-europe.onlinelibrary.wiley.com/doi/10.1002/ejic.202500170 by Ruhr-Universitat Bochum, Wiley Online Library on [04/06/2025]. See the Terms and Conditions (https://onlinelibrary.wiley.com/terms-and-conditions) on Wiley Online Library for rules of use; OA articles are governed by the applicable Creative Commons License

Accepted Manuscript

$[Co^{III}_4O_4]^{4+}/[Co^{IV}Co^{III}_3O_4]^{5+}$ couple, and E2 at around 1.4 V, which can be assigned to the $[Co^{IV}Co^{III}_3O_4]^{5+}/[Co^{IV}_2Co^{III}_2O_4]^{6+}$ couple, in agreement with literature values.[28] This suggests that the oxidation of the $[Co^{III}_4O_4]$ core gives access to Co^{IV}-oxo intermediates, however, the charge is expected to be delocalized over all cobalt atoms. These higher oxidation states of metals are discussed in many catalytic OER cycles at Co_3O_4 spinel catalysts,[9,45] demonstrating that tetranuclear heterocubane-type complexes with a $[Co^{III}_4O_4]$ core can indeed serve as a functional mimic of heterogeneous spinel-type Co_3O_4 OER catalysts. We interpret the small hump at 0.85 V in the anodic scan as ligand oxidation, in accordance with the literature.[46]

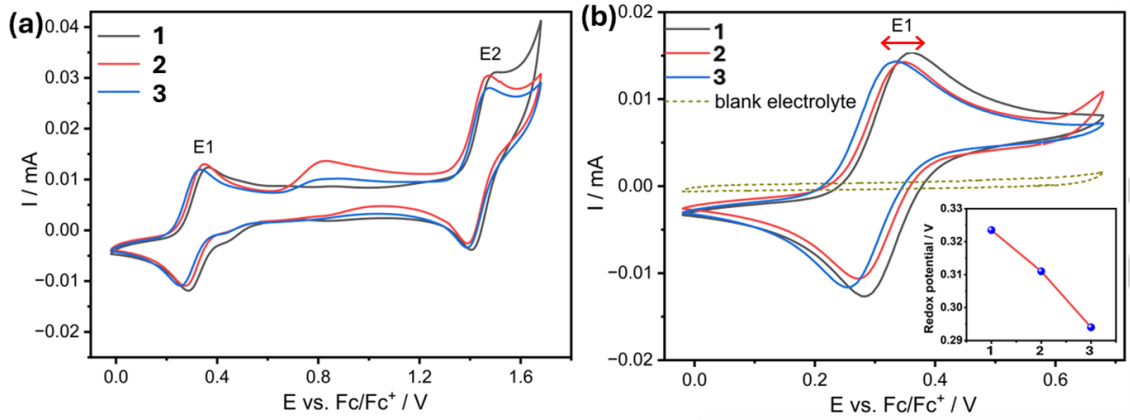


Figure 7. Cyclic voltamogramms of 1 mM cubane complex in 0.1M $TBAPF_6$/MeCN obtained at glassy carbon (GC) electrode at 100 mVs^{-1} over a wider (**a**) and shorter (**b**) potential window. Inset: variation of the formal redox potential of E1 for different complexes. The potential was normalized against Fc/Fc^+ internal redox couple.

Interestingly, the redox potentials of E1 and E2 were slightly but steadily shifted to lower potentials with increasing length of the alkyl chain of the carboxylate ligand, as presented in the correlation plot shown in the inset of **Figure 7**b. The formal redox potential of peak E1 for complexes **1**, **2** and **3** were 0.324, 0.311 and 0.294 V vs. Fc/Fc^+, respectively. This trend of lowering the redox potential by lengthening the alkyl chain may be related to differences in the solvent effect and the stabilization of charged species. We note that the redox shift is rather small, which is expected as the change in the ligand size is just from $-CH_2$ to $-CH_2CH_2CH_3$ and not a substantial substitution or branching of the ligand. Furthermore, the effect of the scan rate on the redox behavior of oxo-cubanes was studied, as presented in Figure S26. Data were analyzed by plotting the peak current (I_p) versus the square root of the scan rate ($u^{1/2}$) (Randles-Sevcik plot). The graphs (Figure S26d) showed excellent linearity with R^2 of 0.9999, suggesting a diffusion-limited process. The plots are almost identical for the three different complexes, which is anticipated for a small change in the molecular size of the complexes. The diffusion coefficient (D) was estimated using Randles-Sevcik analysis and the obtained average diffusion coefficient (D) of the three complexes in TBA^+/MeCN electrolyte is $(7.5 \pm 0.3) \times 10^{-6}$ cm^2 s^{-1}.

In addition, the electrochemical behavior of the trinuclear complex **4** was studied by cyclic voltammetry (Figure S27a). Within the same investigated potential range, the CV of complex **4** shows a different voltammetric behavior from the tetranuclear cubane complexes, e.g. complex **1**, where only an irreversible oxidation peak occurs at about 1.41 V vs. Fc/Fc^+, close to the potential of the second oxidation peak of complex **1**. However, in a larger potential window, the CV of complex **4** shows additional oxidation and reduction peaks (Figure S27b). From studying different potential windows, one can correlate the reduction peak C2 to oxidation peak A2, while C1 is related to A1. Peaks A1 and A2 can be attributed to oxidation of Co(III) to Co(IV), and peaks C1 and C2 are probably due to reduction to Co(III) and possibly even to Co(II). Similar interpretation, though for different peak potentials, was reported for other Co complexes.[47,48] Moreover, the peak potential was shifted with increasing the scan rate, suggesting a kinetically controlled irreversible process (Figure S27c). To this end, such structure-reactivity correlations can provide a guide for the rational design of oxo cubanes and open a new avenue for accessing higher oxidation state Co(IV) intermediate, that can be highly active for catalyzing reactions such as oxygen evolution reaction.

Conclusions

A series of neutral tetranuclear Co(III) carboxylate complexes $[Co_4O_4(O_2CR)_4(py)_4]$ (R = Me **1**, Et **2**, *n*-Pr **3**) with a central heterocubane-type $[Co^{III}_4O_4]$ core as well as trinuclear complexes $[Co^{III}_3(\mu_3\text{-}O)(\mu_2\text{-}OH)(O_2CR)_3(py)_5](NO_3)_2$

This article is protected by copyright. All rights reserved.

10990682c, ja, Downloaded from https://chemistry-europe.onlinelibrary.wiley.com/doi/10.1002/ejic.202500170 by Ruhr-Universitat Bochum, Wiley Online Library on [04/06/2025]. See the Terms and Conditions (https://onlinelibrary.wiley.com/terms-and-conditions) on Wiley Online Library for rules of use; OA articles are governed by the applicable Creative Commons License

Accepted Manuscript

(R = *i*-Pr **4**, *t*-Bu **5**) with a central dicationic [$Co^{III}_3(\mu_3\text{-}O)(\mu_2\text{-}OH)$] core were synthesized and spectroscopically characterized ($^1H/^{13}C$ NMR, FT-IR), while their structures in the solid state were determined by sc-XRD. The gas phase structure of $[Co_4O_4(OAc)_4(py)_4]$ (**1**) was determined by use of quantum chemical calculations and Mayer bond indices were calculated to investigate the electronic structure of **1** in more detail. The DFT simulated IR spectrum of **1** agrees well with the experimental spectrum and allowed for a distinctive assignment of the ligand-based and Co-oxo based modes. Electronic transitions in the tetranuclear complexes as determined using UV/Vis spectroscopy are consistent with computational results based on density functional theory (DFT). Furthermore, the electrochemical properties of complex **1**−**4** are compared. CV measurements revealed (quasi-)reversible redox peaks of all complexes with slightly decreasing redox potentials with increasing carbon chain length of the ligand, and the isolation and structural characterization of as-formed oxidation products is currently under investigation.

Experimental Section

Materials and Reagents

All reagents were commercially available and used without further purification. Synthesis of all complexes followed a modified procedure of Chakrabarty et al.[17]

Synthesis of Complexes 1 − 5

$[Co_4O_4(OAc)_4(py)_4]$ (1). $Co(NO_3)_2{\cdot}6H_2O$ (10 mmol, 2.9 g) and NaOAc (20 mmol, 1.6 g) were dissolved in 30 mL of MeOH. After heating the solution to reflux, pyridine (10 mmol, 0.8 mL) and 30% H_2O_2 (50 mmol, 5 mL) were slowly added, and the purple mixture immediately turned dark green. The solution was heated to reflux for additional 4 h. After half of the solvent was removed at reduced pressure, 20 mL of DCM were added. The resulting dark green organic phase was collected and dried with $MgSO_4$. Half of the solvent was then removed at reduced pressure, and the product was precipitated with petroleum ether. After drying at reduced pressure, a dark green powder was obtained. Single crystals were grown by slow evaporation of the solvent from a solution of 1 in DCM. Yield: 77% based on Cobalt. Anal. calcd. for $C_{28}H_{32}O_{12}N_4Co_4$ (852 g mol^{-1}) C: 39.46%; H: 3.78%; N: 6.57%; Co: 27.66%. Found: C: 38.8 %; H: 3.84%; N: 6.64%; Co: 28.1%. ^1H NMR (400 MHz, D_2O) δ 8.27 (d, $^3J_{H\text{-}H}$ = 5.2 Hz, 8 H, py o-H), 7.80 (m, 4 H, py p-H), 7.29 (dd, $^3J_{H\text{-}H}$ = 7.6; $^3J_{H\text{-}H}$ = 6.5 Hz, 8 H, py m-H), 2.30 – 1.99 (s, 12 H, $OOCH_3$). ^{13}C NMR (101 MHz, D_2O) δ 188.84 (s, OOC), 151.99 (s, py o-C), 138.94 (s, py p-C), 124.88 (s, py m-C), 25.60 (s, CH_3).

$[Co_4O_4(O_2CEt)_4(py)_4]$ (2). The synthesis was performed similar to that of **1**, but replacing NaOAc by NaO_2CEt (20 mmol, 1.924 g). Since 2 did not precipitate after the addition of petroleum ether, 2 was purified by column chromatography (silica column) and a mixture of cHex/EtOH (2.5:1). The first fraction was collected, and after removing the solvent at reduced pressure, a dark green powder was obtained. Single crystals were obtained by vapor diffusion of *n*-hexane into a solution of 2 in DCM. Yield: 45.5% based on Cobalt. Anal. calcd. for $C_{32}H_{40}O_{12}N_4Co_4$ (908 g mol^{-1}) C: 42.31%; H: 4.44%; N: 6.17%; Co: 25.95%. Found: C: 41.71 %; H: 4.59%; N: 5.98%; Co: 26.4%. ^1H NMR (400 MHz, D_2O) δ 8.28 (dd, $^3J_{H\text{-}H}$ = 6.3; $^4J_{H\text{-}H}$ = 1.3 Hz, 8 H, py o-H), 7.80 – 7.74 (m, 4 H, py p-H), 7.27 (dd, $^3J_{H\text{-}H}$ = 7.6; $^3J_{H\text{-}H}$ = 6.5 Hz, 8 H, py m-H), 2.47 – 2.31 (q, $^3J_{H\text{-}H}$ = 7.5 Hz, 8 H, CH_2), 1.06 (t, $^3J_{H\text{-}H}$ = 7.6 Hz, 12H, CH_3). ^{13}C NMR (101 MHz, D_2O) δ 191.97 (s, OOC), 152.07 (s, py o-C), 138.79 (s, py p-C), 124.79 (s, py m-C), 32.57 (s, CH_2), 9.52 (s, CH_3).

$[Co_4O_4(O_2C$*n*$\text{-Pr})_4(py)_4]$ (3). The synthesis was analogously performed with NaO_2CPr (20 mmol, 2.255 g), resulting in the isolation of a dark green powder. Single crystals were obtained by vapor diffusion of *n*-hexane into a solution of 3 in DCM. Yield: 9.3% based on Cobalt. Anal. calcd. for $C_{36}H_{48}O_{12}N_4Co_4$ (964 g mol^{-1}) C: 44.83%; H: 5.02%; N: 5.81%; Co: 24.44%. Found: C: 44.81 %; H: 5.24%; N: 5.66%; Co: 24.73%. ^1H NMR (400 MHz, D_2O) δ 8.29 (dd, $^3J_{H\text{-}H}$ = 6.4 Hz; $^4J_{H\text{-}H}$ = 1.4 Hz 8 H, py o-H), 7.77 (tt, $^3J_{H\text{-}H}$ = 7.7 Hz; $^4J_{H\text{-}H}$ = 1.5 Hz 4 H, py p-H), 7.27 (dd, $^3J_{H\text{-}H}$ = 7.6; $^3J_{H\text{-}H}$ 6.5 Hz, 8 H, py m-H), 2.38 – 2.30 (m, 8 H, $OOCCH_2$), 1.57 (m, 8 H, CH_2), 0.91 – 0.86 (t, $^3J_{H\text{-}H}$ = 7.4 Hz, 12 H, CH_3). ^{13}C NMR (101 MHz, D_2O) δ 191.38 (s, OOC), 152.19 (s, py o-C), 138.84 (s, py p-C), 124.82 (s, py m-C), 41.51 (s, OOC$\underline{C}H_2$), 19.07 (s, $\underline{C}H_2CH_3$), 13.32 (s, CH_3).

$[Co^{III}_3(\mu_3\text{-}O)(\mu_2\text{-}OH)_2(O_2C$*i*$\text{-Pr})_3(py)_5]^{2+}$ $2NO_3^-$ (4). The synthesis was performed similar to that of **1** but replacing NaOAc by NaO_2C*i*-Pr (20 mmol, 2.200 g). Since **4** did not precipitate after the addition of petroleum ether nor cHex, 4 was purified by washing with THF. Resulting in the isolation of a dark green powder. Single crystals were obtained by vapor diffusion of *n*-hexane into a solution of 4 in THF. Yield: 2.37% based on Cobalt. Anal. calcd. for $C_{35}H_{52}O_{13}N_3Co_3$ (899,61 g*mol^{-1}) C: 46.73%; H: 5.83%; N: 4.67%; Co: 19.65%. Found: C: 44.00%; H: 5.68%; N: 4.42%; Co: 20.70%. ^1H NMR (400 MHz, CD_3CN) δ 8.52 (dd, $^3J_{H\text{-}H}$ = 6.4; $^4J_{H\text{-}H}$ = 1.3 Hz, 2H, py o-H), 8.43 (d, $^3J_{H\text{-}H}$

This article is protected by copyright. All rights reserved.

10990682c, ja, Downloaded from https://chemistry-europe.onlinelibrary.wiley.com/doi/10.1002/ejic.202500170 by Ruhr-Universität Bochum, Wiley Online Library on [04/06/2025]. See the Terms and Conditions (https://onlinelibrary.wiley.com/terms-and-conditions) on Wiley Online Library for rules of use; OA articles are governed by the applicable Creative Commons License

Accepted Manuscript

= 5.2 Hz, 4H, py o-H), 8.05 – 7.95 (m, 3H, 2 py p-H), 7.88 (s, 4H, py o-H), 7.63 (t, $^3J_{H-H}$ = 7.6 Hz, 2H, py p-H), 7.58 – 7.51 (m, 6H, 2 py m-H), 7.15 (t, $^3J_{H-H}$ = 6.9 Hz, 4H), 2.96 (hept, $^3J_{H-H}$ = 7.0 Hz, 1H, OOCCH), 2.70 (hept, $^3J_{H-H}$ = 7.0 Hz, 2H, OOCCH), 1.43 (s 2H, OH) 1.15 (d, $^3J_{H-H}$ = 7.0 Hz, 6H, CH_3), 1.10 (d, $^3J_{H-H}$ = 7.0 Hz, 6H, CH_3), 1.05 (d, $^3J_{H-H}$ = 6.9 Hz, 6H, CH_3). ^{13}C NMR (101 MHz, CD_3CN) δ 195.07 (s, OOC), 193.70 (s, OOC), 153.36 (s, py o-C), 153.09 (s, py o-C), 152.54 (s, py o-C), 140.51 (s, py p-C), 140.26 (s, py p-C), 125.93 (s, py m-C), 125.66 (s, py m-C), 38.89 (s, CH), 38.01 (s, CH), 19.83 (s, CH_3), 19.61 (s, CH_3), 19.55 (s, CH_3).

$[Co^{III}_3(\mu_3\text{-}O)(\mu_2\text{-}OH)_2(O_2C\textit{t}\text{-}Bu)_3(py)_5]^{2+}$ $2NO_3^-$ (5). The synthesis was performed similar to that of **1** but replacing NaOAc by NaO_2C*t*-Bu (16,5 mmol, 2,050g). Single crystals were obtained by slow vapor diffusion of *n*-hexane into a solution of 5 in THF. Complex 5 only formed as minor product in all experiments, while the major component turned out to be the known complex $[Co^{III}_3(\mu_3\text{-}O)(\mu_2\text{-}OH)(OOC\textit{t}\text{-}Bu)_5(py)_3]^+$ NO_3^- initially reported by Das et al..[36]

Spectroscopic Characterization

IR spectra were collected on a Bruker ALPHA-P FT-IR with a single reflection ATR sample head. IR measurements were performed in a glovebox under argon atmosphere. UV/Vis spectra were recorded on a Shimadzu UV-2600i spectrophotometer.

Cyclic voltammetry (CV) studies

CV measurements were conducted using an Autolab PGSTAT204 potentiostat/galvanostat in a three-electrode setup comprising a GC (3 mm diameter) working electrode, Pt sheet as the counter electrode and Ag/AgCl (3M KCl) as the reference electrode. Prior to recording CVs, the GC electrode was polished with alumina slurry (3.0, 1.0, 0.05 µm in a descending order) on lapping cloths (Buehler, USA). The electrodes were then rinsed with acetone and water and dried under air flow. The potentials were converted to a scale vs. Fc/Fc^+, where its formal potential was experimentally determined in the same studied electrolyte.

Single-crystal X-ray diffraction.

Crystals were mounted on nylon loops in inert oil. Data were collected on a Bruker AXS D8 Kappa diffractometer with APEX2 detector (mono-chromated $Mo_{K\alpha}$ radiation, λ = 0.71073 Å) at 100(2) K. Those of **4** were collected on a Bruker AXS D8 Venture diffractometer with Photon II detector (mono-chromated $Cu_{K\alpha}$ radiation, λ = 1.54178 Å, mircofocus source) at 100(2) K. The structures were solved by Direct Methods (SHELXS-2013)[49] and refined anisotropically by full-matrix least-squares on F^2 (SHELXL-2017).[50] Absorption corrections were performed semi-empirically from equivalent reflections on basis of multi-scans (Bruker AXS APEX3). Hydrogen atoms were refined using a riding model or rigid methyl groups.

The OH hydrogen atom in **2** was refined freely with its O–H bond lengths restrained to be equal to 0.85 Å (DFIX). In **2** and **4** the OH hydrogen atoms' displacement parameters were coupled to the ones of the corresponding O, while those in **5** were refined freely without any con- or restraints.

The structure of **2** contains two dichloromethane molecules of which one is disordered over two sites. The corresponding bond lengths and angles were restrained to be equal (SADI) and RIGU restrained were used in the refinement of the displacement parameters. A methanol and an *n*-pentane molecule are disordered over a center of inversion. The local symmetry was ignored in the refinement of the pentane (negative PART). The bond lengths and angles of the pentane molecule were restrained to be equal (SADI). Its displacement parameters were constrained to be equal and equal to those of the carbon atom of the methanol which is in close proximity (EADP) and strongly correlated. In addition, an ethyl group is disordered over two positions. The crystal was twinned and the model refined as a 2-component pseudo-merohedral twin (TWIN, BASF). A separate integration of the components failed due to overlapping. Despite the small contribution of the minor component (approx. 3%) the *R*-values are significantly reduced.

In **3** a dichloromethane molecule is disordered over two positions. Due to the close proximity the alternate positions of the atoms were refined with common displacement parameters (EADP). The displacement ellipsoids of the other solvent molecule suggest minor disorder but a refinement with split positions failed. During the measurement ice formed on the crystals and the resulting diffraction may have distorted individual reflection intensities.

This article is protected by copyright. All rights reserved.

10990682c, ja, Downloaded from https://chemistry-europe.onlinelibrary.wiley.com/doi/10.1002/ejic.202500170 by Ruhr-Universität Bochum, Wiley Online Library on [04/06/2025]. See the Terms and Conditions (https://onlinelibrary.wiley.com/terms-and-conditions) on Wiley Online Library for rules of use; OA articles are governed by the applicable Creative Commons License

Accepted Manuscript

An anion and the solvent molecule of **4** are disordered. They could be crudely modelled by two alternate positions however their displacement parameters suggest further disorder which could not be resolved. The corresponding bond lengths and angles were restrained to be equal (SADI) and RIGU restraints were applied to the displacement parameters. In case of the nitrate additional SIMU restraints were used and due to their close proximity, the nitrogens' displacement parameters were constrained to be equal (EADP).

In **5** a *t*-butyl group and a nitrate are disordered over two positions. The bond lengths and angles of all nitrate ions were restrained to be equal and RIGU restraints were applied to their displacement parameters. Due to their close proximity the displacement parameters of N1_1 and N1_7 were constrained to be equal (EADP). The corresponding bond lengths and angles of the solvent molecules were restrained to be equal (SADI) and RIGU and SIMU restraints were applied to their displacement parameters. Three of them were too disordered to be modelled properly. The final refinement was done with a dataset from a PLATON/SQUEEZE run were these molecules had been removed.[51] The molecules were included in the sum formula for completeness. The model was refined as a two-component inversion twin.

CCDC-2392548 (**2**), -2392549 (**3**) -2430856 (**4**), and -2430857 (**5**) contain contain the supplementary crystallographic data for this paper. These data can be obtained free of charge from The Cambridge Crystallographic Data Centre via www.ccdc.cam.ac.uk/data_request/cif.

Computational Details

All DFT calculations were done with the TURBOMOLE program package (version 7.8)[52,53] employing the resolution-of-the-identity (RI) approximation. Unless further specified, geometries were optimized in vacuum using RI-DFT (modules ridft and rdgrad)[54–56] with the PBE0[57–59] functional in the def2-SVP basis set[55,60] with the m5 grid[54] and a self-consistent field (SCF) energy convergence threshold of 10^{-8}. All molecular structures together with their DFT energies are available from the “Computational Data.zip” file as part of the Supporting Information. Final properties of complex **1** (i.e., bond indices and spectra) were calculated at a geometry with tighter convergence thresholds, both for the MOs (SCF energy convergence: 10^{-10}) and during the structure optimization (energy convergence: 10^{-9}; Cartesian gradient convergence: 10^{-4}), with grid 5 in the def2-TZVP[55,60] basis set. Mayer bond indices[61] were calculated with the proper module. IR absorption spectra were calculated using analytic Hessians for the harmonic frequencies (with the aoforce module).[62] To model the experimental UV/Vis absorption spectra of complex **1** in solution, vertical electronic excitation energies (VEEs) and oscillator strengths were calculated using TDDFT (using the escf module)[63,64] with the PBE0 functional and the def2-TZVP basis set. To account for solvation effects on the VEEs, the implicit solvent model COSMO (Conductor-like screening model)[65] with settings for acetonitrile (relative dielectric constant $\epsilon_r = 37.5$ and refractive index $n = 1.344$) was used.

For the stability analysis of the tetra- vs. trinuclear complexes, differences in the Gibbs free energy in solution (G_{tot}) were calculated. Geometries for all species have been optimized at the finer PBE0/def2-TZVP level of theory with tightened convergence criteria (*vide supra*). The final DFT energy in vacuum was used as the electronic contribution (E_{el}) to G_{tot}. The thermal contributions (E_{th}) have been calculated using the rigid-rotor–harmonic-oscillator model at 25 °C (using freeh) based on the harmonic frequencies calculated at the DFT level.

Gibbs free energies of solvation (δG_{solv}) were calculated with the conductor-like screening model for real solvents (COSMO-RS) at the BP-TZVPD-FINE level of theory as implemented in COSMO*therm* (version 2021).[66] For these calculations, the geometries were re-optimized with the BP86[67,68] functional in the def-TZVP basis set[55,60] in both vacuum and in the so-called conductor-limit (i.e., assuming $\epsilon = \infty$ for the dielectric constant) of COSMO.[65] Details on COSMO and COSMO-RS as well as the precise computational protocol for δG_{solv} can be found elsewhere.[69,70] A temperature of 25 °C and a molar fraction of 100 % for the solvent (methanol, diethyl ether, tetrahydrofuran, cyclohexane) and vanishing concentrations (x = 0) for the complexes as solutes were used. Finally, the total Gibbs free energy of each species at 25 °C in solution (G_{tot}) was obtained as a sum of the electronic, thermal, and solvation contributions as individually described above:

$$G_{tot} = E_{el} + E_{th} + \delta G_{solv} \quad (3)$$

Supporting Information

The Supporting Information is available free of charge at: LINK

This article is protected by copyright. All rights reserved.

10990682c, ja, Downloaded from https://chemistry-europe.onlinelibrary.wiley.com/doi/10.1002/ejic.202500170 by Ruhr-Universitat Bochum, Wiley Online Library on [04/06/2025]. See the Terms and Conditions (https://onlinelibrary.wiley.com/terms-and-conditions) on Wiley Online Library for rules of use; OA articles are governed by the applicable Creative Commons License

Accepted Manuscript

Experimental spectra, calculated spectra, crystallographic details, electrochemical data, calculated transition orbitals.

Acknowledgements

We acknowledge support from the University of Duisburg-Essen (S.S.). We are thankful for Beate Römer for elemental analyses, Julian Grahl for the UV/Vis measurement and Joana Tewes for the lab work support.

Corresponding Author

* Stephan Schulz, Institute of Inorganic Chemistry and CENIDE, University of Duisburg-Essen, 45141 Essen, Germany. ORCID 0000-0003-2896-4488; Email: stephan.schulz@uni-due.de

Author Contributions

T. Fockenberg − Synthesis, Characterization, Writing manuscript draft. N. Sülzner − DFT calculations. H. Amin – Electrochemical measurements, Writing and Revision. C. Wölper − sc-XRD measurements. C. Hättig − Supervision, Manuscript Revision. S. Schulz – Conceptualization, Supervision, Project administration, Manuscript Revision. The manuscript was written through contributions of all authors. All authors have given approval to the final version of the manuscript.

Funding Sources

Financial support by the Deutsche Forschungsgemeinschaft (DFG; German Research Foundation, Project no. 388390466) within the Collaborative Research Center/Transregio CRC/TRR 247 “Heterogeneous Oxidation Catalysis in the Liquid Phase” (Projects C03, A05).

Keywords: Cobalt (III) carboxylates • sc-XRD • Cyclic voltammetry • DFT calculations

References

[1] F. Cavani, J. H. Teles, ”Sustainability in Catalytic Oxidation: An Alternative Approach or a Structural Evolution?” *ChemSusChem* **2009**, *2*, 508.

[2] R. Matheu, P. Garrido-Barros, M. Gil-Sepulcre, M. Z. Ertem, X. Sala, C. Gimbert-Suriñach, A. Llobet, ”The Development of Molecular Water Oxidation Catalysts” *Nat. Rev. Chem.* **2019**, *3*, 331.

[3] J. Song, C. Wei, Z. F. Huang, C. Liu, L. Zeng, X. Wang, Z. J. Xu, “A Review on Fundamentals for Designing Oxygen Evolution Electrocatalysts” *Chem. Soc. Rev.* **2020**, *49*, 2196.

[4] S. Saddeler, U. Hagemann, S. Schulz, “Effect of the Size and Shape on the Electrocatalytic Activity of Co_3O_4Nanoparticles in the Oxygen Evolution Reaction” *Inorg. Chem.* **2020**, *59*, 10013.

[5] D. Waffel, E. Budiyanto, T. Porske, J. Büker, T. Falk, Q. Fu, S. Schmidt, H. Tüysüz, M. Muhler, B. Peng, “Investigation of Synergistic Effects between Co and Fe in $Co_{3-x}Fe_xO_4$ Spinel Catalysts for the Liquid-Phase Oxidation of Aromatic Alcohols and Styrene” *Mol. Catal.* **2020**, *498*, 111251.

[6] T. Falk, E. Budiyanto, M. Dreyer, C. Pflieger, D. Waffel, J. Büker, C. Weidenthaler, K. F. Ortega, M. Behrens, H. Tüysüz, M. Muhler, B. Peng, “Identification of Active Sites in the Catalytic Oxidation of 2-Propanol over $Co_{1+x}Fe_{2-x}O_4$ Spinel Oxides at Solid/Liquid and Solid/Gas Interfaces” *ChemCatChem* **2021**, *13*, 2942.

[7] T. Falk, S. Anke, H. Hajiyani, S. Saddeler, S. Schulz, R. Pentcheva, B. Peng, M. Muhler, “Influence of the Particle Size on Selective 2-Propanol Gas-Phase Oxidation over Co_3O_4 Nanospheres” *Catal. Sci. Technol*. **2021**, *11*, 7552.

[8] J. Amtawong, A. I. Nguyen, T. D. Tilley, “Mechanistic Aspects of Cobalt–Oxo Cubane Clusters in Oxidation Chemistry” *J. Am. Chem. Soc.* **2022**, *144*, 1475.

[9] A. I. Nguyen, M. S. Ziegler, P. Oña-Burgos, M. Sturzbecher-Hohne, W. Kim, D. E. Bellone, T. D. Tilley, “Mechanistic Investigations of Water Oxidation by a Molecular Cobalt Oxide Analogue: Evidence for a Highly Oxidized Intermediate and Exclusive Terminal Oxo Participation” *J. Am. Chem. Soc.* **2015**, *137*, 12865.

This article is protected by copyright. All rights reserved.

10990682c, ja, Downloaded from https://chemistry-europe.onlinelibrary.wiley.com/doi/10.1002/ejic.202500170 by Ruhr-Universität Bochum, Wiley Online Library on [04/06/2025]. See the Terms and Conditions (https://onlinelibrary.wiley.com/terms-and-conditions) on Wiley Online Library for rules of use; OA articles are governed by the applicable Creative Commons License

Accepted Manuscript

[10] F. Song, R. Moré, M. Schilling, G. Smolentsev, N. Azzaroli, T. Fox, S. Luber, G. R. Patzke, "{Co_4O_4} and {$Co_xNi_{4-x}O_4$} Cubane Water Oxidation Catalysts as Surface Cut-Outs of Cobalt Oxides" *J. Am. Chem. Soc.* **2017**, *139*, 14198.

[11] M. D. Symes, Y. Surendranath, D. A. Lutterman, D. G. Nocera, "Bidirectional and Unidirectional PCET in a Molecular Model of a Cobalt-Based Oxygen-Evolving Catalyst" *J. Am. Chem. Soc.* **2011**, *133*, 5174.

[12] P. F. Smith, C. Kaplan, J. E. Sheats, D. M. Robinson, N. S. McCool, N. Mezle, G. C. Dismukes, "What Determines Catalyst Functionality in Molecular Water Oxidation? Dependence on Ligands and Metal Nuclearity in Cobalt Clusters" *Inorg. Chem*. **2014**, *53*, 2113.

[13] X. Li, E. B. Clatworthy, A. F. Masters, T. Maschmeyer, "Molecular Cobalt Clusters as Precursors of Distinct Active Species in Electrochemical, Photochemical, and Photoelectrochemical Water Oxidation Reactions in Phosphate Electrolytes" *Chem. Eur. J.* **2015**, *21*, 16578.

[14] J. K. Beattie, T. W. Hambley, J. A. Klepetko, A. F. Masters, P. Turner, "The chemistry of cobalt acetate - IV. The isolation and crystal structure of the symmetric cubane, tetrakis[(μ-acetato)(μ_3-Oxo) (pyridine)cobalt(III)] chloroform solvate, [Co_4(μ-O)$_4$(μ-CH_3CO_2)$_4$(C_5H_5N) $_4$] 5$CHCl_3$ and of the dicationic partial cubane, trimeric, [(μ-acetato)(acetato)tris(μ-hdyroxy(μ_3-oxo) hexakispyridinetricobalt(III)]hexafluorophosphate water solvate, [Co_3(μ_3-O)(μ-OH)$_3$(μ-CH_3CO_2(CH_3CO_2(C_5H_5N)$_6$[PF_6]2 2H_2O" *Polyhedron* **1998**, *17*, 1343.

[15] R. Chakrabarty, B. K. Das, "Epoxidation of α-Pinene Catalysed by Tetrameric Cobalt(III) Complexes" *J. Mol. Catal. A Chem*. **2004**, *223*, 39.

[16] B. K. Das, J. H. Clark, "A Novel Immobilised Cobalt(III) Oxidation Catalyst" *Chem. Commun.* **2000**, *7*, 605.

[17] R. Chakrabarty, S. J. Bora, B. K. Das, "Synthesis, Structure, Spectral and Electrochemical Properties, and Catalytic Use of Cobalt(III)-Oxo Cubane Clusters" *Inorg. Chem*. **2007**, *46*, 9450.

[18] R. Chakrabarty, D. Kalita, B. K. Das, "Catalytic Oxidation of P-Xylene in Water by Cobalt(III) Cubane Cluster" *Polyhedron* **2007**, *26*, 1239.

[19] B. K. Das, R. Chakrabarty, "Cobalt(III)-Oxo Cubane Clusters as Catalysts for Oxidation of Organic Substrates" *J. Chem. Sci*. **2011**, *123*, 163.

[20] R. Chakrabarty, P. Sarmah, B. Saha, S. Chakravorty, B. K. Das, "Catalytic Properties of Cobalt(III)-Oxo Cubanes in the TBHP Oxidation of Benzylic Alcohols" *Inorg. Chem.* **2009**, *48*, 6371.

[21] P. Sarmah, R. Chakrabarty, P. Phukan, B. K. Das, "Selective Oxidation of Alcohols Catalysed by a Cubane-like Co(III) Oxo Cluster Immobilised on Porous Organomodified Silica" *J. Mol. Catal. A Chem*. **2007**, *268*, 36.

[22] R. Chakrabarty, B. K. Das, J. H. Clark, "Enhanced Selectivity in Green Catalytic Epoxidation Using a Supported Cobalt Complex" *Green Chem*. **2007**, *9*, 845.

[23] P. Sarmah, B. K. Das, "Catalysis of TBHP Oxidation of Styrene and Diphenylmethane by a Supported Cobalt(III)-Oxo Cluster" *Indian J. Chem. Sect. A*. **2014**, *53*, 41.

[24] J. G. McAlpin, T. A. Stich, C. A. Ohlin, Y. Surendranath, D. G. Nocera, W. H. Casey, R. D. Britt, "Electronic Structure Description of a [$Co(III)_3Co(IV)O_4$] Cluster: A Model for the Paramagnetic Intermediate in Cobalt-Catalyzed Water Oxidation" *J. Am. Chem. Soc*. **2011**, *133*, 15444.

[25] R. G. Hadt, D. Hayes, C. N. Brodsky, A. M. Ullman, D. M. Casa, M. H. Upton, D. G. Nocera, L. X. Chen, "X-Ray Spectroscopic Characterization of Co(IV) and Metal-Metal Interactions in Co_4O_4: Electronic Structure Contributions to the Formation of High-Valent States Relevant to the Oxygen Evolution Reaction" *J. Am. Chem. Soc.* **2016**, *138*, 11017.

[26] C. N. Brodsky, R. G. Hadt, D. Hayes, B. J. Reinhart, N. Li, L. X. Chen, D. G. Nocera, "In Situ Characterization of Cofacial Co(IV) Centers in Co_4O_4 Cubane: Modeling the High-Valent Active Site in Oxygen-Evolving Catalysts" *PNAS*. **2017**, *114*, 3855.

[27] J. Amtawong, B. B. Skjelstad, D. Balcells, T. D. Tilley, "Concerted Proton-Electron Transfer Reactivity at a Multimetallic Co_4O_4 Cubane Cluster" *Inorg. Chem*. **2020**, *59*, 15553.

[28] A. I. Nguyen, J. Wang, D. S. Levine, M. S. Ziegler, T. D. Tilley, "Synthetic Control and Empirical Prediction of Redox Potentials for Co_4O_4 Cubanes over a 1.4 v Range: Implications for Catalyst Design and Evaluation of High-Valent Intermediates in Water Oxidation" *Chem. Sci.* **2017**, *8*, 4274.

This article is protected by copyright. All rights reserved.

10990682c, ja, Downloaded from https://chemistry-europe.onlinelibrary.wiley.com/doi/10.1002/ejic.202500170 by Ruhr-Universität Bochum, Wiley Online Library on [04/06/2025]. See the Terms and Conditions (https://onlinelibrary.wiley.com/terms-and-conditions) on Wiley Online Library for rules of use; OA articles are governed by the applicable Creative Commons License

Accepted Manuscript

[29] M. W. Ishaq, R. Nawaz, A. Jalil, M. A. Hashmi, T. Zheng, L. Li, "Ligand Exchange Reaction in [Co_4O_4]-Cobalt Cubane: A Versatile Strategy Towards the Preparation of Cobalt Cubane-Based Functional Small Molecules and Polymeric Materials" *J. Mol. Struct*. **2021**, **1235**, 130216.

[30] S. Berardi, G. La Ganga, M. Natali, I. Bazzan, F. Puntoriero, A. Sartorel, F. Scandola, S. Campagna, M. Bonchio, "Photocatalytic Water Oxidation: Tuning Light-Induced Electron Transfer by Molecular Co_4O_4 Cores" *J. Am. Chem. Soc*. **2012**, *134*, 11104.

[31] Y. Wang, F. Li, X. Zhou, F. Yu, J. Du, L. Bai, L. Sun, "Highly Efficient Photoelectrochemical Water Splitting with an Immobilized Molecular Co_4O_4 Cubane Catalyst" *Angew. Chem. Int. Ed*. **2017**, *56*, 6911; *Angew. Chem.* **2017**, *129*, 7015.

[32] Z. Luo, Y. Hou, J. Zhang, S. Wang, X. Wang, "Beilstein Bioinspired Cobalt Cubanes with Tunable Redox Potentials for Photocatalytic Water Oxidation and CO_2 Reduction" *Beilstein J. Org. Chem*. **2018**, *14*, 2331.

[33] S. Gutiérrez-Tarriño, J. Gaona-Miguélez, P. Oña-Burgos, "Tailoring the Electron Density of Cobalt Oxide Clusters to Provide Highly Selective Superoxide and Peroxide Species for Aerobic Cyclohexane Oxidation" *Dalton Trans*. **2021**, *50*, 15370.

[34] F. Evangelisti, R. Güttinger, R. Moré, S. Luber, G. R. Patzke, "Closer to Photosystem II: A Co_4O_4 Cubane Catalyst with Flexible Ligand Architecture" *J. Am. Chem. Soc*. **2013**, *135*, 18734.

[35] A. Scheurer, J. Korzekwa, T. Nakajima, F. Hampel, A. Buling, C. Derks, M. Neumann, L. Joly, K. Petukhov, K. Gieb, P. Müller, K. Kuepper, K. Meyer, "Synthesis, Magnetic Properties, and X-Ray Spectroscopy of Divalent Cobalt(II) and Nickel(II) Cubanes [$M^{II}_4(HL_2)_4(OAc)_4$]" *Eur. J. Inorg. Chem*. **2015**, 1892.

[36] S. J. Bharali, B. K. Das, "A Synthetic Approach to Trinuclear Cluster with [$Co_3(\mu_3\text{-}O)(\mu\text{-}OH)$] Core: A Comparative Study on Cluster Having [$Co_3(\mu_3\text{-}O)(\mu\text{-}OH)$] and [$Co_4(\mu_3\text{-}O)_4$] Core" *Z. Anorg. Allg. Chem*. **2021**, *647*, 794.

[37] J. K. Beattie, J. A. Klepetko, A. F. Masters, P. Turner, "The Chemistry of Cobalt Acetate. VIII. New Members of the Family of Oxo-Centred Trimers, See Abstract" *Polyhedron* **2003**, *22*, 947.

[38] C. E. J. Sumner, "Interconversion of Dinuclear and Oxo-Centered Trinuclear Cobaltic Acetates" *Inorg. Chem.* **1988**, *27*, 1320.

[39] Q. Zeng, F. W. Lewis, L. M. Harwood, F. Hartl, "Role of Ligands in Catalytic Water Oxidation by Mononuclear Ruthenium Complexes" *Coord. Chem. Rev*. **2015**, *304–305*, 88.

[40] D. W. Crandell, S. Xu, J. M. Smith, M. H. Baik, "Intramolecular Oxyl Radical Coupling Promotes O-O Bond Formation in a Homogeneous Mononuclear Mn-Based Water Oxidation Catalyst: A Computational Mechanistic Investigation" *Inorg. Chem*. **2017**, *56*, 4435.

[41] C. J. Richmond, S. Escayola, A. Poater, "Axial Ligand Effects of Ru-BDA Complexes in the O–O Bond Formation via the I2M Bimolecular Mechanism in Water Oxidation Catalysis" *Eur. J. Inorg. Chem.* **2019**, 2101.

[42] S. A. Chavan, D. Srinivas, P. Ratnasamy, "Selective Oxidation of *para*-Xylene to Terephthalic Acid by μ_3-Oxo-Bridged Co/Mn Cluster Complexes Encapsulated in Zeolite–Y" *J. Catal*. **2001**, *204*, 409.

[43] H. J. Eppley, H.-L. Tsai, N. De Vries, K. Felting, G. Christou, D. N. Hendrickson, "High-Spin Molecules: Unusual Magnetic Susceptibility Relaxation Effects in [$Mn_{12}O_{12}(O_2CEt)_{16}(H_2O)_3$] (S = 9) and the One-Electron Reduction Product (PPh_4)[$Mn_{12}O_{12}(O_2CEt)_{16}(H_2O)_4$] (S = $^{19}/_2$)" *J. Am. Chem. Soc.* **1995**, *117*, 301.

[44] T. G. Mayerhöfer, S. Pahlow, J. Popp, "The Bouguer-Beer-Lambert Law: Shining Light on the Obscure" *ChemPhysChem*. **2020**, *21*, 2029.

[45] T. C. Davenport, H. S. Ahn, M. S. Ziegler, T. D. Tilley, "A Molecular Structural Analog of Proposed Dinuclear Active Sites in Cobalt-Based Water Oxidation Catalysts" *Chem. Commun*. **2014**, *50*, 6326.

[46] S. Li, Z. Zhang, W. R. Marks, X. Huang, H. Chen, D. C. Stoian, R. Erni, C. A. Triana, G. R. Patzke, "{Co_4O_4} Cubanes in a conducting polymer matrix as bio-inspired molecular oxygen evolution catalysts" *Nat. Commun*. **2024**, *15*, 8432.

[47] M. Masahiro, N. Yuko, I. Ayumi, O. Mika, Y. Daisuke, S. Hiroshi, H. Makoto, T. Motohiro, "Mixed-Valent Trinuclear Co^{III}-Co^{II}-Co^{III} Complex with 1,3-Bis(5-Chlorosalicylideneamino)-2-Propanol" *Molecules* **2022**, *27*, 4211.

This article is protected by copyright. All rights reserved.

10990682c, ja, Downloaded from https://chemistry-europe.onlinelibrary.wiley.com/doi/10.1002/ejic.202500170 by Ruhr-Universität Bochum, Wiley Online Library on [04/06/2025]. See the Terms and Conditions (https://onlinelibrary.wiley.com/terms-and-conditions) on Wiley Online Library for rules of use; OA articles are governed by the applicable Creative Commons License

Accepted Manuscript

[48] M. Mikuriya, Y. Naka, D. Yoshioka, M. Handa, "Synthesis and Crystal Structures of Dinuclear Cobalt(III) Complexes with 1,3-Bis(5-Nitrosalicylideneamino)-2-Propanol and 1,3-Bis(3-Nitrosalicylideneamino)- 2-Propanol" *X-ray Struct. Anal. Online* **2016**, *32*, 55.

[49] G. M. Sheldrick, "Phase Annealing in SHELX-90: Direct Methods for Larger Structures" *Acta Crystallogr.* **1990**, *A46*, 467.

[50] G. M. Sheldrick, "Crystal Structure Refinement with SHELXL" *Acta Crystallogr. Sect. C Struct. Chem*. **2015**, *71*, 3.

[51] P. Van Der Sluis, A. L. Spek," BYPASS: an effective method for the refinement of crystal structures containing disordered solvent regions" *Acta Crystallogr.* **1990**, *A46*, 194.

[52] TURBOMOLE V7.8 2023, a development of University of Karlsruhe and Forschungszentrum Karlsruhe GmbH, 1989-2007, TURBOMOLE GmbH, since 2007; available from https://www.turbomole.org.

[53] Y. J. Franzke, C. Holzer, J. H. Andersen, T. Begušić, F. Bruder, S. Coriani, F. Della Sala, E. Fabiano, D. A. Fedotov, S. Fürst, S. Gillhuber, R. Grotjahn, M. Kaupp, M. Kehry, M. Krstić, F. Mack, S. Majumdar, B. D. Nguyen, S. M. Parker, F. Pauly, A. Pausch, E. Perlt, G. S. Phun, A. Rajabi, D. Rappoport, B. Samal, T. Schrader, M. Sharma, E. Tapavicza, R. S. Treß, V. Voora, A. Wodyński, J. M. Yu, B. Zerulla, F. Furche, C. Hättig, M. Sierka, D. P. Tew, F. Weigend, "TURBOMOLE: Today and Tomorrow" *J. Chem. Theory Comput.* **2023**, *19*, 6859.

[54] K. Eichkorn, F. Weigend, O. Treutler, R. Ahlrichs, "Auxiliary Basis Sets for Main Row Atoms and Transition Metals and Their Use to Approximate Coulomb Potentials" *Theor. Chem. Acc.* **1997**, *97*, 119.

[55] K. Eichkorn, O. Treutler, H. Öhm, M. Häser, R. Ahlrichs, "Auxiliary Basis Sets to Approximate Coulomb Potentials" *Chem. Phys. Lett.* **1995**, *242*, 652.

[56] O. Treutler, R. Ahlrichs, "Efficient Molecular Numerical Integration Schemes" *J. Chem. Phys.* **1995**, *102*, 346.

[57] J. P. Perdew, Y. Wang, "ASM Metals Reference Book" *Phys. Rev. Lett.* **1994**, *45*, 13244.

[58] J. P. Perdew, K. Burke, M. Ernzerhof, "Generalized Gradient Approximation Made Simple" *Phys. Rev. Lett.* **1996**, *77*, 3865.

[59] J. P. Perdew, M. Ernzerhof, K. Burke, "Rationale for Mixing Exact Exchange with Density Functional Approximations" *J. Chem. Phys.* **1996**, *105*, 9982.

[60] F. Weigend, R. Ahlrichs, "Balanced Basis Sets of Split Valence, Triple Zeta Valence and Quadruple Zeta Valence Quality for H to Rn: Design and Assessment of Accuracy" *Phys. Chem. Chem. Phys.* **2005**, *7*, 3297.

[61] I. Mayer, "Bond Order and Valence Indices: A Personal Account" *J. Comput. Chem.* **2007**, *28*, 204.

[62] P. Deglmann, K. May, F. Furche, R. Ahlrichs, "Nuclear Second Analytical Derivative Calculations Using Auxiliary Basis Set Expansions" *Chem. Phys. Lett.* **2004**, *384*, 103.

[63] R. Bauernschmitt, R. Ahlrichs, "Treatment of Electronic Excitations within the Adiabatic Approximation of Time Dependent Density Functional Theory" *Chem. Phys. Lett.* **1996**, *256*, 454.

[64] R. Bauernschmitt, M. Häser, O. Treutler, R. Ahlrichs, "Calculation of Excitation Energies within Time-Dependent Density Functional Theory Using Auxiliary Basis Set Expansions" *Chem. Phys. Lett.* **1997**, *264*, 573.

[65] A. Schäfer, A. Klamt, D. Sattel, J. C. W. Lohrenz, F. Eckert, "COSMO Implementation in TURBOMOLE: Extension of an Efficient Quantum Chemical Code towards Liquid Systems" *Phys. Chem. Chem. Phys.* **2000**, *2*, 2187.

[66] BIOVIA COSMO*therm*, Release , Dassault Systèmes, https://www.3ds.com.

[67] A. D. Becke, "Density-Functional Exchange-Energy Approximation with Correct Asymptotic Behavior" *Phys. Rev. A* **1988**, *38*, 3098.

[68] J. P. Perdew, "Density-Functional Approximation for the Correlation Energy of the Inhomogeneous Electron Gas" *Phys. Rev. B* **1986**, *33*, 8822.

[69] A. Hellweg, F. Eckert, "Brick by Brick Computation of the Gibbs Free Energy of Reaction in Solution Using Quantum Chemistry and COSMO-RS" *AIChE J.* **2017**, *63*, 3944.

This article is protected by copyright. All rights reserved.

10990682c, ja, Downloaded from https://chemistry-europe.onlinelibrary.wiley.com/doi/10.1002/ejic.202500170 by Ruhr-Universität Bochum, Wiley Online Library on [04/06/2025]. See the Terms and Conditions (https://onlinelibrary.wiley.com/terms-and-conditions) on Wiley Online Library for rules of use; OA articles are governed by the applicable Creative Commons License

Accepted Manuscript

10.1002/ejic.202500170

[70] A. Klamt, “The COSMO and COSMO-RS Solvation Models” *WIREs Comput Mol Sci* **2018**, *8*, 1.

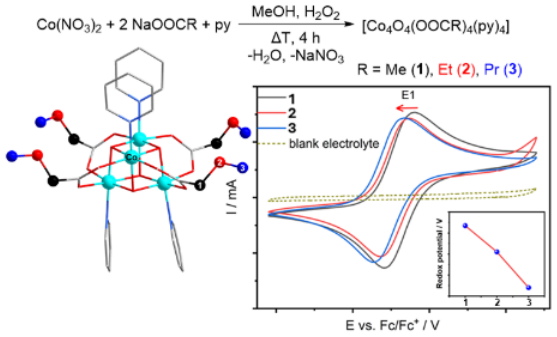
Accepted Manuscript

10990682c, ja, Downloaded from https://chemistry-europe.onlinelibrary.wiley.com/doi/10.1002/ejic.202500170 by Ruhr-Universitat Bochum, Wiley Online Library on [04/06/2025]. See the Terms and Conditions (https://onlinelibrary.wiley.com/terms-and-conditions) on Wiley Online Library for rules of use; OA articles are governed by the applicable Creative Commons License

This article is protected by copyright. All rights reserved.

10.1002/ejic.202500170

Entry for the Table of Contents



A series of three tetranuclear and two trinuclear Co(III) carboxylate complexes were synthesized and characterized by sc-XRD, NMR, IR and UV/vis spectroscopy as well as by cyclovoltammetrie (CV). The relative stability of the tetranuclear vs. trinuclear complexes was investigated by DFT calculations and the IR and UV/Vis spectra were calculated to deconvolute contributions of the tetranuclear and trinuclear Co-oxo core from those of the organic ligands, respectively.

This article is protected by copyright. All rights reserved.

10990682c, ja, Downloaded from https://chemistry-europe.onlinelibrary.wiley.com/doi/10.1002/ejic.202500170 by Ruhr-Universitat Bochum, Wiley Online Library on [04/06/2025]. See the Terms and Conditions (https://onlinelibrary.wiley.com/terms-and-conditions) on Wiley Online Library for rules of use; OA articles are governed by the applicable Creative Commons License